





# Regulatory NADH dehydrogenase-like complex optimizes C<sub>4</sub> photosynthetic carbon flow and cellular redox in maize

Qiqi Zhang<sup>1,2</sup>, Shilong Tian<sup>2</sup>, Genyun Chen<sup>1</sup>, Qiming Tang<sup>1,2</sup>, Yijing Zhang<sup>3</sup> , Andrew J. Fleming<sup>4</sup> ,  
Xin-Guang Zhu<sup>1</sup>  and Peng Wang<sup>1</sup> 

<sup>1</sup>CAS Center for Excellence in Molecular Plant Sciences, Institute of Plant Physiology and Ecology, Chinese Academy of Sciences, Shanghai, China; <sup>2</sup>University of Chinese Academy of Sciences, Beijing, China; <sup>3</sup>State Key Laboratory of Genetic Engineering, Collaborative Innovation Center of Genetics and Development, Department of Biochemistry, Institute of Plant Biology, School of Life Sciences, Fudan University, Shanghai, 200438, China; <sup>4</sup>School of Biosciences, University of Sheffield, Western Bank, Sheffield, S10 2TN, UK

## Summary

Author for correspondence:  
Peng Wang  
Email: [wangpeng@cemps.ac.cn](mailto:wangpeng@cemps.ac.cn)

Received: 18 March 2023  
Accepted: 20 September 2023

New Phytologist (2023)  
doi: 10.1111/nph.19332

**Key words:** bundle sheath cell, C<sub>4</sub> photosynthesis, CO<sub>2</sub> concentration mechanism, cyclic electron transport, maize, NDH complex, photosynthetic metabolite, redox regulation.

- C<sub>4</sub> plants typically operate a CO<sub>2</sub> concentration mechanism from mesophyll (M) cells into bundle sheath (BS) cells. NADH dehydrogenase-like (NDH) complex is enriched in the BS cells of many NADP-malic enzyme (ME) type C<sub>4</sub> plants and is more abundant in C<sub>4</sub> than in C<sub>3</sub> plants, but to what extent it is involved in the CO<sub>2</sub> concentration mechanism remains to be experimentally investigated.
- We created maize and rice mutants deficient in NDH function and then used a combination of transcriptomic, proteomic, and metabolomic approaches for comparative analysis.
- Considerable decreases in growth, photosynthetic activities, and levels of key photosynthetic proteins were observed in maize but not rice mutants. However, transcript abundance for many cyclic electron transport (CET) and Calvin–Benson cycle components, as well as BS-specific C<sub>4</sub> enzymes, was increased in maize mutants. Metabolite analysis of the maize *ndh* mutants revealed an increased NADPH:NADP ratio, as well as malate, ribulose 1,5-bisphosphate (RuBP), fructose 1,6-bisphosphate (FBP), and photorespiration intermediates.
- We suggest that by optimizing NADPH and malate levels and adjusting NADP-ME activity, NDH functions to balance metabolic and redox states in the BS cells of maize (in addition to ATP supply), coordinating photosynthetic transcript abundance and protein content, thus directly regulating the carbon flow in the two-celled C<sub>4</sub> system of maize.

## Introduction

Plants use light energy to drive CO<sub>2</sub> assimilation into carbohydrates through photosynthesis. Rice and wheat are the most widely consumed food crops, but the C<sub>3</sub> photosynthesis in these plants does not operate in an efficient way, with the assimilation of CO<sub>2</sub> considerably compromised due to photorespiration (Bauwe *et al.*, 2010; Raines, 2011). Crops such as maize and sorghum have evolved a distinct and more efficient process, C<sub>4</sub> photosynthesis. Typical C<sub>4</sub> leaves display a special Kranz anatomy: vascular bundles of C<sub>4</sub> maize leaves are sequentially surrounded by functionally differentiated bundle sheath (BS) cells and mesophyll (M) cells, which contain chloroplasts with different ultrastructure and a specific distribution of metabolic enzymes. In C<sub>4</sub> plants, CO<sub>2</sub> is concentrated through intercellular transport of C<sub>4</sub> acids (such as malate and aspartate) from M cells where CO<sub>2</sub> is captured, to the BS cells where Rubisco is present. The C<sub>4</sub> acids are decarboxylated in the BS cells, raising CO<sub>2</sub> concentration around Rubisco, decreasing photorespiration, and thus achieving more efficient assimilation of CO<sub>2</sub> and improved photosynthesis (Furbank, 2017; von Caemmerer *et al.*, 2017).

Two distinct C<sub>4</sub> subtypes have been classified based on their major decarboxylation enzyme, the NADP-malic enzyme (ME) type and NAD-ME type, both inherently involving a supplementary phosphoenolpyruvate carboxykinase (PEPCK) cycle (Wang *et al.*, 2014). For the NADP-ME type C<sub>4</sub> plant maize, one distinctive feature of BS chloroplasts may be a strong ability to perform cyclic electron transport (CET). Cyclic electron transport pathways are mainly mediated by the chloroplast NADH dehydrogenase-like complex (NDH) and by the proton gradient regulatory proteins, that is proton gradient regulation 5 (PGR5) and PRG5-like photosynthetic phenotype 1 (PGRL1; Johnson, 2011; Shikanai, 2014; Suorsa, 2015; Yamori & Shikanai, 2016). The NDH complex binds to photosystem I (PSI) and is specifically distributed in the nonstacking regions of thylakoids (Kouřil *et al.*, 2014; Yadav *et al.*, 2017). By mediating CET from the receptor side of PSI to plastoquinone (PQ), an NDH-dependent proton gradient is established across the thylakoid membrane to drive ATP synthesis (Wang *et al.*, 2006; Ishikawa *et al.*, 2016b; Strand *et al.*, 2017). In C<sub>3</sub> plants, CET is not prominent under normal conditions, with CO<sub>2</sub> assimilation mainly driven by linear photosynthetic electron transport (LET).

However, under environmental stresses, such as high temperature, high light, and drought, LET is suppressed, while CET via NDH is often upregulated, helping to decrease oxidative damage and to replenish ATP (Burrows *et al.*, 1998; Endo *et al.*, 1999; Horváth *et al.*, 2000; Li *et al.*, 2004; Wang *et al.*, 2006; Ishikawa *et al.*, 2008; Yamori *et al.*, 2011; Suorsa, 2015). In the  $C_4$  plant maize, BS chloroplasts lack the stacking grana thylakoids rich in photosystem II (PSII) and instead possess a large number of non-stacking stromal thylakoids rich in PSI and NDH complex (Majeran & van Wijk, 2009; Ermakova *et al.*, 2020). As the BS-specific upregulation of NDH has been confirmed at both transcript and protein levels (Kubicki *et al.*, 1996; Darie *et al.*, 2005, 2006; Takabayashi *et al.*, 2005; Majeran *et al.*, 2008; Friso *et al.*, 2010; Li *et al.*, 2010; Bräutigam *et al.*, 2011), the functional significance of such enrichment has aroused great interest.

It has been noted that NDH content is higher in a range of  $C_4$  leaves (both NADP-ME and NAD-ME types) than in  $C_3$  leaves, leading to the idea that it provides increased ATP generation required by the  $C_4$  pathway (Ishikawa *et al.*, 2016b). As evidence, studies on several  $C_4$  plants have shown that the NDHH subunit is increased in cell types requiring additional ATP for  $CO_2$  concentration (e.g. BS cells of NADP-ME type and M cells of NAD-ME type leaves; Takabayashi *et al.*, 2005). In some  $C_4$  species, only NDH-mediated CET is enhanced, while in others both NDH and PGR5-PGRL1 pathways are enhanced (Munekage *et al.*, 2010; Nakamura *et al.*, 2013). On the other hand, whether NDH plays other specific role apart from ATP production in the  $C_4$  pathway is unknown. Further functions may be related to the involvement of NDH-CET in NADPH turnover and redox adjustment, and understanding the different redox needs in the M and BS chloroplasts of  $C_4$  plants may be crucial for engineering efficient  $C_4$  photosynthesis (Turkan *et al.*, 2018). In particular, NADP-malic enzyme (NADP-ME) catalyzes the decarboxylation of malate to yield  $CO_2$  and pyruvate with the concomitant production of NADPH (Drincovich *et al.*, 2001), the main source of reducing power for BS chloroplasts in maize. Besides having acquired an enriched BS expression, the  $C_4$ -type NADP-ME displays a particular redox modulation in maize (Alvarez *et al.*, 2012). Whether or how NDH-CET, as well as the ferredoxin/thioredoxin system, are related to this modulation is of great interest.

Studies have found that mutations in the NDHN or NDHO subunits of maize lead to increased photorespiration and reduced carbon assimilation under high-light and saturated  $CO_2$  conditions (Peterson *et al.*, 2016). In the  $C_4$  species *Flaveria bidentis*, knockout of the NDHN or NDHO subunit, but not PGR5 or PGRL1, resulted in slow plant growth and decreased  $CO_2$  assimilation (Ishikawa *et al.*, 2016a; Ogawa *et al.*, 2023). These studies indicate that NDH is crucial for photosynthesis and growth of  $C_4$  plants (at least in the NADP-ME subtype), but the mechanism underlying the phenotype remains to be elucidated. In this study, we took a reverse genetic approach and created mutants of selected NDH subunits (NDF6 and NDHU subunits), both in a NADP-ME subtype  $C_4$  crop (maize) and a  $C_3$  crop (rice), and then used a combination of transcriptomic, proteomic, and metabolomic approaches to identify the mechanism by which loss of NDH activity in  $C_4$  leaves leads to decreased  $CO_2$  assimilation

and growth. Our data highlight the importance of BS-localized NDH activity in maize for the balancing of carbon flux and redox state between the BS and M cells. The necessity of this regulation is most prominent in the BS cells, which undergo continuous import of malate and generation of NADPH as an essential part of the  $C_4$  mechanism.

## Materials and Methods

### Plant growth conditions and trait measurement

Maize (*Zea mays* ssp. *mays* KN5585) plants were grown in 6 l pots with a mix of 60% peat soil and 20% vermiculite. Rice (*Oryza sativa* L. cv ZhongHua11) plants were grown in 6 l pots with field soil. The plants were grown in environmentally controlled phytotron room (27°C:25°C, day: night, 600  $\mu\text{mol photons m}^{-2} \text{s}^{-1}$  photosynthetic photon flux density (PPFD), 16 h : 8 h, light : dark photoperiod, and c. 70% relative humidity) with normal fertilizer application.

To estimate leaf total chlorophyll content, a SPAD 502 Plus Chlorophyll Meter (Konica Minolta Sensing, Osaka, Japan) was used. Plant height was measured from the soil surface to the collar of the youngest fully expanded leaf.

### Blue native (BN)-polyacrylamide gel electrophoresis (PAGE) and Western blot

For BN-PAGE, thylakoid membranes were separated from maize leaves, solubilized with 1.2% (w/v) *n*-dodecyl- $\beta$ -maltoiside (DDM), and subjected to Native-PAGE. Excised BN-PAGE lanes were soaked in SDS sample buffer and layered onto 12.5% SDS polyacrylamide gels for two-dimensional analysis. Immunoblot analysis was performed according to standard procedure. See Supporting Information Methods S1 for detailed process.

### Monitoring chlorophyll fluorescence and P700 redox

Postillumination increase in chlorophyll fluorescence was monitored after turning off the actinic light (200  $\mu\text{mol photons m}^{-2} \text{s}^{-1}$ , white light, for 180 s), using a PAM chlorophyll fluorometer (PAM101; Walz, Effeltrich, Germany) attached with emitter-detector assembly and 101ED unit, as described previously (Wang *et al.*, 2006). Fv/Fm, ETR, and NPQ were measured using a PAM-2000 chlorophyll fluorometer (Walz) according to standard procedures.

The redox kinetics of P700 was recorded using a Dual-PAM-100 instrument (Walz). Before measurements, the leaves were dark-acclimated for 20 min. Far-red light (30 s) was applied to start the measurement, and the initial rate of  $P700^+$  reduction following termination of far-red light was calculated.

### Photosynthetic gas exchange measurements

The photosynthetic rate of phytotron-grown plants 60 d after transplanting was measured using LI-6800 (for maize) or LI-6400 (for rice) portable gas exchange systems (Li-Cor

Biosciences, Lincoln, NE, USA). The temperature, relative humidity, and PPFD were set at 28°C, 70%, and 1200  $\mu\text{mol m}^{-2} \text{s}^{-1}$ , respectively, for the leaf chamber.  $\text{CO}_2$  concentrations were set as 400, 200, 50, 100, 150, 200, 300, 400, 500, 600, 800, 1000, and 1200 ppm in a stepwise manner. The  $A/C_i$  curve of maize was fitted according to Zhou *et al.* (2019).

### Transmission electron microscopy

Maize leaf sections of 2 mm were fixed in 2.5% glutaraldehyde, postfixed in osmium tetroxide, and embedded in Spurr's resin, and ultra-thin sections were imaged at 80 kV with a Hitachi H-7650 transmission electron microscope (Hitachi High-tech, Tokyo, Japan). See Methods S2 for more details.

### Histological staining of ROS accumulation

Leaf fragments of 2 cm were stained with DAB staining solution (1 mg  $\text{ml}^{-1}$  DAB, 10 mM  $\text{Na}_2\text{HPO}_4$ , and 0.05% Tween-20) and then processed with paraffin sectioning, and cross sections were examined with light microscopy. See Methods S3 for more details.

### Paraffin section and $\text{I}_2$ -KI staining

Leaf sections were dissected and fixed in formaldehyde-acetic acid-alcohol (FAA) solution, processed with standard paraffin sectioning protocol as described in Methods S4, and starch was visualized by iodine potassium iodide ( $\text{I}_2$ -KI) staining.

### RNA sequencing

For maize, leaves at the youngest fully expanded stage were sampled, from 30-d-old plants. And for rice, samples were harvested from 60-d-old plants. Both maize and rice leaves were sampled at c. 10:00 h with liquid nitrogen. Each biological replicate consisted of leaves from four individual plants, and three biological replicates (from 12 plants in total) were sequenced for each sample. Library preparation followed standard procedure, and the libraries were sequenced on Illumina Novaseq 6000 platform using 150-bp paired-end sequencing strategy. The cleaned reads of maize samples were mapped onto the Zm-B73-REFERENCE-NAM-5.0 reference genome, and cleaned reads of rice samples were mapped onto the RAP Gene ID reference genome, both using HISAT2. The differentially expressed genes (DEGs) were identified by DESeq2 (v.1.16.1) with definition of fold change  $> 2$  and false discovery rate (FDR)  $< 0.01$ . See Datasets S1, S2 for the original transcriptome data of maize and rice and Dataset S3 for a summary of transcript abundance of photosynthetic genes.

### Transcript abundance analysis

RNA extraction, cDNA synthesis, and qRT-PCR were carried out using commercial kits as detailed in Methods S5. Relative transcript abundance was calculated by comparison with *ZmEF1 $\alpha$*  (Hughes & Langdale, 2020).

### Separation of BS strands

Bundle sheath strands were isolated using a method modified from Chang *et al.* (2012), as described in Methods S6. Each biological replicate for the following mass spectrometry analysis consisted of leaves from six individual plants, and three biological replicates were used for each sample.

### Mass spectrometry analysis of protein samples

Equal amount of proteins (20  $\mu\text{g}$ ) were used for mass spectrometry analysis. See Methods S7 for detailed sample processing. Relative protein amounts and the fold changes in *zmndf6* mutant relative to the wild-type (WT) were presented. See Dataset S4 for the original BS cell proteomics results.

### Metabolite profiling

Maize and rice samples were harvested at c. 10:00 h from the same stages of plants used for RNA-seq. Each biological replicate consisted of four leaf disks (diameter = 8 mm) from one individual plant, and at least six biological replicates (six plants from three different mutant lines) were prepared for measurement. For each biological replicate, four leaf disks (c. 40 mg) were flash-frozen (dropped into liquid nitrogen within 1 s after cutting) and ground in a tissue grinding machine, 30 Hz  $\times$  1 min, three times. The ground powder was mixed with 800  $\mu\text{l}$  extraction buffer (methanol : chloroform = 7 : 3 (v/v),  $-20^\circ\text{C}$  precooled), shaken in the tissue grinding machine (30 Hz for 3 min), and the mixture was kept in  $-20^\circ\text{C}$  for 3–4 h. The mixture was added with 560  $\mu\text{l}$  cold distilled water, shaken in the tissue grinding machine (30 Hz for 5 min), and put back in  $-20^\circ\text{C}$  for 10 min. The sample was centrifuged at 2200 g, for 10 min at  $4^\circ\text{C}$ , and the supernatant (c. 800  $\mu\text{l}$ ) was transferred to a new tube and kept in  $-20^\circ\text{C}$ . For a 2<sup>nd</sup> extraction, 800  $\mu\text{l}$  of 50% methanol was added to the pellet and the tube was carefully vortexed for 15 s before put back in  $-20^\circ\text{C}$ . After 30 min, it was centrifuged again at 2200 g, for 10 min at  $4^\circ\text{C}$ , and the supernatant (c. 800  $\mu\text{l}$ ) was combined with last extraction. The total supernatant (c. 1.6 ml) was filtered by 0.22  $\mu\text{m}$  filter, and 5  $\mu\text{l}$  was injected for HPLC-MS/MS analysis or for quality control.

Luna NH2 column (3  $\mu\text{m}$ , 100 mm  $\times$  2 mm; Phenomenex Co. Ltd, Torrance, CA, USA) was used in liquid chromatography, and the separation was conducted with a gradient set of solution A (20 mM Ammonium acetate in 5% acetonitrile solution, adjusted to pH 9.5 with ammonia water) and solution B (acetonitrile): 0–1 min, 15% A and 85% B; 1–8 min, 70% A and 30% B; 8–22 min, 95% A and 5% B; 22–25 min, 15% A and 85% B. Mass spectrometry analysis of the eluent was performed with QTRAP 6500+ (AB Sciex Co. Ltd, Framingham, MA, USA) in multireaction monitoring (MRM) mode, parameters (could be found in Dataset S5) were referred from previous work (Tang *et al.*, 2022), and data analysis was performed using Analyst<sup>®</sup> 1.6 software. Metabolites detected were identified by aligning the retention time to features of standard samples processed on the same platform. The relative amounts of each

metabolite in different samples were calculated by the chromatographic peak areas, and the changes in the metabolites relative to the averaged values of the WT were presented. We have checked in the pilot experiments to ensure that the amount of samples we injected (dilute when necessary) resulted in values within the linear range. The data presentation was adopted from Li *et al.* (2020).

## Results

### Construction of NDF6 and NDHU subunit deficient mutants in maize and rice

Chloroplast NDH is structurally divided into five subcomplexes: A, B, M (membrane), L (lumen), and ED (electron donor; Fig. S1a). Subcomplex B is composed of five subunits (PnsB1-5) and is specific to chloroplast NDH (Shikanai, 2016; Ma *et al.*, 2021). By data mining, we found that the transcript abundance of *NDF6* (gene assigned as *PnsB4* recently) and *NDHU* (NDHU belongs to subcomplex ED) in maize BS cells was higher than in M cells and higher in maize leaves than in rice leaves (Fig. S1b; Table S1; Li *et al.*, 2010; Wang *et al.*, 2014). In addition, their upregulation amplitude in maize leaves relative to rice leaves was much higher than that of *NDHN* and *NDHO*, which had been targeted in previously reported maize mutants (Peterson *et al.*, 2016), while *PGR5* and *PGRL1* transcripts were not highly accumulated in maize leaves compared with rice leaves (Fig. S1b; Table S1). The transcript levels of *NDF6*, *NDHN*, and *NDHO* were relatively comparable in rice leaves (Fig. S1c). To dissect and compare the significance of NDH-mediated CET in  $C_4$  and  $C_3$  photosynthesis, we generated maize and rice loss-of-function mutants of *NDF6* and *NDHU* subunits using CRISPR-Cas9 technology.

For maize *ndh* mutants, two sgRNAs each were designed for the near 5'-terminal sequences of the first exons of *ZmNDF6* and *ZmNDHU* genes to construct gene editing vectors. Seven *ZmNDF6*-edited and 5 *ZmNDHU*-edited maize plants were obtained. Three lines with 49, 51, and 54-bp homozygous deletions (starting at 16 bp after ATG) in the *ZmNDF6* gene were named *zmndf6-1*, *zmndf6-2*, and *zmndf6-3*, respectively. Two homozygous mutation types in *ZmNDHU* (*zmndhu-1* and *zmndhu-2*) were also identified (Figs S1a, S2a,c).

For *ndh* mutants in rice, single sgRNAs near the 5' ends of the third exon of the *OsNDF6* gene and the first exon of the *OsNDHU* gene were designed, respectively, to construct gene editing vectors. Twelve *OsNDF6*-edited rice plants were obtained, including three *osndf6* homozygous lines with 3 or 10-bp deletions or a single base insertion. They were named *osndf6-1*, *osndf6-2*, and *osndf6-3*, respectively. Seven *OsNDHU*-edited samples were sequenced but all T0 plants were found to be heterozygous. After segregation, we identified homozygous *osndhu* mutants with a single A-base insertion or 163-bp deletion and named them *osndhu-1* and *osndhu-2*, respectively (Figs S1c, S2b,d).

The changes in NDH protein components between the mutants and WT were analyzed by Western blot. As expected, the *NDF6* subunit was almost undetectable in the leaves of the

*zmndf6* (Fig. 1e), and the NDHU subunit in *zmndhu* could barely be detected (Fig. 1f). The protein levels of NDHH, NDHS, and NDHO subunits were also decreased in the maize *ndh* mutants (Fig. 1e,f). The decrease in these subunits likely affected the amount and assembly of the NDH-PSI supercomplex as well, as reflected by blue native gel and a 2<sup>nd</sup>-dimension electrophoresis (Fig. 1i,j). By detecting the subunits of PSI, PSII, cytochrome b6f, and ATP synthase, we found that the protein level of the PsaA but not the PsaD subunit tended to be lower in *zmndf6*, while the PsaD but not the PsaA subunit tended to be lower in *zmndhu* than in WT. The protein level of PsaA (D1) was lower in both *zmndf6* and *zmndhu* than in WT, while the PetA subunit of cytochrome b6f complex and the AtpB subunit of ATP synthase were not notably different from that of the WT (Fig. S4b,c, see later). Protein levels of the NDH subunits tested were also much decreased in the rice *osndf6* and *osndhu* mutants (Fig. 1g,h), but compared with the situation in the maize mutants, protein levels related to PSI, PSII, cytochrome b6f, and ATP synthase were not notably changed in the rice mutants (only PsaD and PsaA showed a slight downward trend; Fig. S4d,e, see later).

### Retarded growth of *ndf6* and *ndhu* mutants in maize but not in rice despite decreased cyclic electron flow in both

After 30-d culture of T1 plants in a phytotron, the growth of *zmndf6* and *zmndhu* mutants was retarded compared with that of the WT maize KN5585 (Fig. 1a). Leaf chlorophyll contents and plant height of *zmndf6* and *zmndhu* mutants were significantly lower ( $P < 0.01$ ) than those of the WT (Fig. 1b). The yellowish leaf color of T1 plants was more obvious after 30 d in a field glasshouse than in the phytotron (Fig. S3). Slower growth and reduced pigment levels were also observed in maize transposon insertion mutants of *ndhn* and *ndho* (Peterson *et al.*, 2016). However, rice *osndf6* and *osndhu* mutants showed no obvious difference in growth and chlorophyll content compared with their WT ZH11 (Fig. 1c,d).

Postillumination increase in chlorophyll fluorescence is used to indicate the operation of CET. When the driving force of LET via PSII is absent, NDH complex-mediated electrons from the receptor side of PSI can flow back to reduce the intersystem PQ pool, causing a recovery in PSII chlorophyll fluorescence level (Asada *et al.*, 1993; Mano *et al.*, 1995; Mi *et al.*, 1995). Compared with the WT, the postillumination increase in chlorophyll fluorescence disappeared in maize *zmndf6* and *zmndhu* mutants, demonstrating that the activity of CET was inhibited (Fig. 2a). Similar results were found in the *ndhn* and *ndho* mutants of maize, although the postillumination increase was not fully diminished (Peterson *et al.*, 2016). In addition, the decline of the chlorophyll fluorescence induction curve under actinic light was slower in the mutants than that in WT, indicating a state of over-reduction of the electron transport chain (Fig. S4a). Far-red light induces an increase in 810–830 nm absorption (representing oxidation of P700), and the activity of CET around PSI is partially reflected by a decrease in the light absorption (representing reduction of P700<sup>+</sup>) after turning off the far-red light



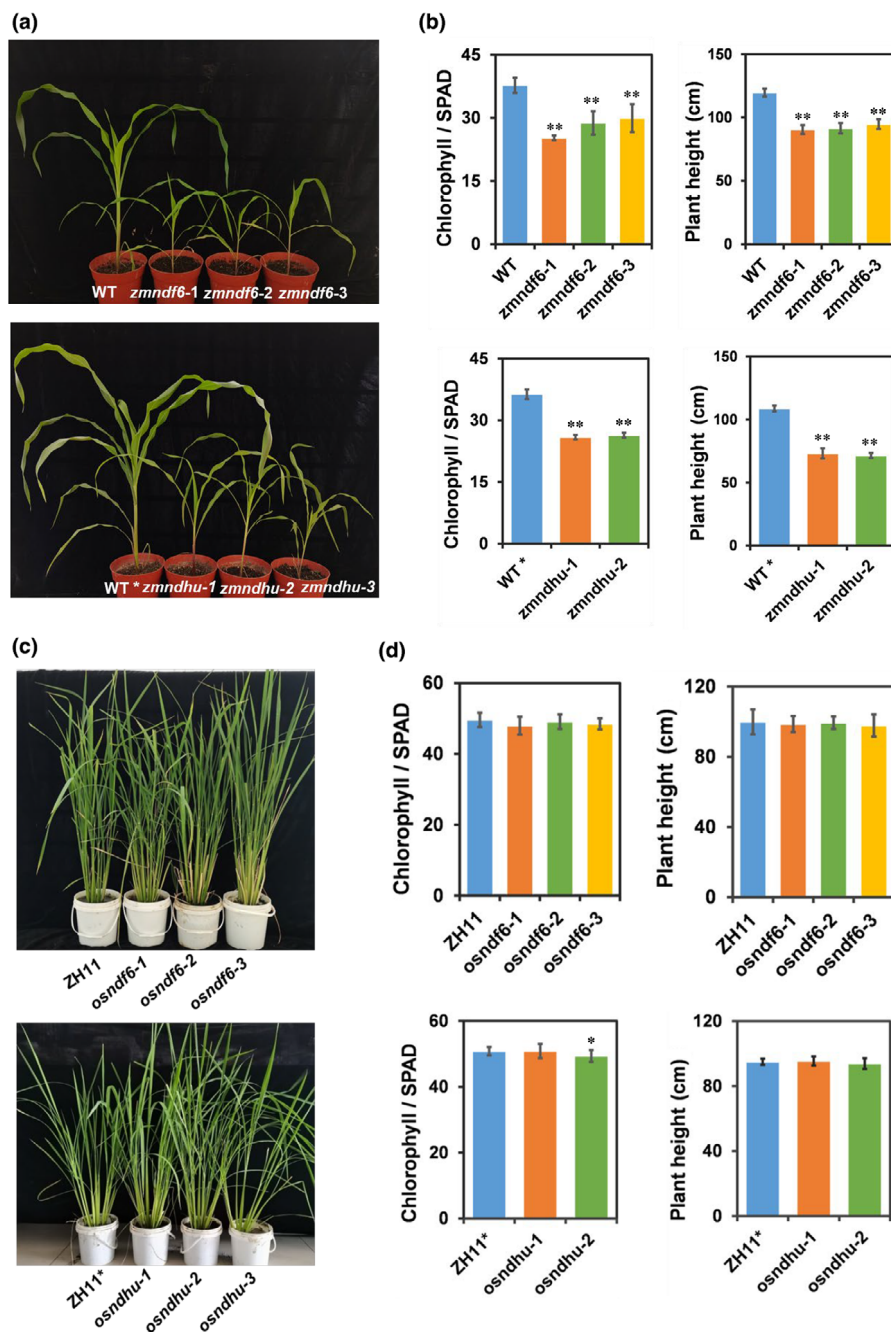


**Fig. 1** Altered growth phenotype in maize but not in rice *ndh* mutants. (a) Maize plants of WT (KN5585) and *ndh* mutants 30 d after planting. (b) Comparisons of chlorophyll content and plant height between wild-type (WT) and *ndh* mutants. Data are mean  $\pm$  SE ( $n = 6$  biological replicates for chlorophyll content and plant height). (c) Rice plants of WT (ZH11) and *ndh* mutants 60 d after planting. (d) Comparisons of chlorophyll content and plant height between WT and *ndh* mutants. Data are mean  $\pm$  SE ( $n = 12$  and eight biological replicates for chlorophyll content and plant height, respectively). \*,  $P < 0.05$ ; \*\*,  $P < 0.01$  compared with WT according to Student's *t*-test. (e–h) Western blots showing the protein changes in NDH subunits between maize KN5585 and *zmndf6* mutants (e), maize KN5585 and *zmndhu* mutants (f), rice ZH11 and *osndf6* mutants (g), and rice ZH11 and *osndhu* mutants (h). (i) Thylakoid membrane protein complexes isolated from WT, *zmndf6*, and *zmndhu* were solubilized and separated by BN-PAGE (5–12%). High-molecular-weight green bands specific to WT are indicated. (j) Thylakoid membrane protein complexes separated by BN-PAGE were subjected to 2<sup>nd</sup> dimension SDS-PAGE (12.5%), and the proteins were immunodetected with specific antibodies against NDHS, and NDHH, respectively. The red arrows indicates the NDH-PSI supercomplex (i) or distribution of NDHH protein (j). WT\* indicates the WT used in a different batch together with *zmndhu* mutants, and ZH11\* indicates the WT used in a different batch together with *osndhu* mutants, due to timing and availability of transgenic materials.

(Maxwell & Biggins, 1976; Asada *et al.*, 1992; Mi *et al.*, 1992). The dark reduction rate of  $P700^+$  in *zmndf6* and *zmndhu* mutants was significantly lower ( $P < 0.01$  or  $< 0.05$ ) than that of the WT (Fig. 2b), indicating the partial inactivation of CET.

In rice *osndf6* and *osndhu* leaves, compared with the WT the postillumination increase in chlorophyll fluorescence was decreased in *osndf6* and *osndhu* mutants (Fig. 2a), but (unlike in maize) there was no major difference in the descending phase of chlorophyll fluorescence under actinic light. The  $P700^+$  reduction rate of *osndf6* and *osndhu* mutants decreased to different degrees compared with that of the WT (Fig. 2b). These results show that the activity of the CET pathway was also impeded in the rice NDH-deficient mutants.

Photosynthetic light reaction and  $CO_2$  assimilation are severely impaired in maize but not in rice NDH-deficient mutants

To explore whether and to what extent the photosynthetic activity of NDH-deficient  $C_4$  and  $C_3$  plants was affected, we tested the  $CO_2$  response curve ( $A/C_i$ ), electron transfer rate (ETR), nonphotochemical quenching (NPQ), and other photosynthetic parameters of the maize and rice mutants. It was found that the initial slopes of the  $A/C_i$  curve and the level of steady-state photosynthetic rate were clearly lower in maize *zmndf6* and *zmndhu* mutants than those in the maize WT (Fig. 3a,b), as were the levels of ETR and NPQ in *zmndf6* and *zmndhu* mutants

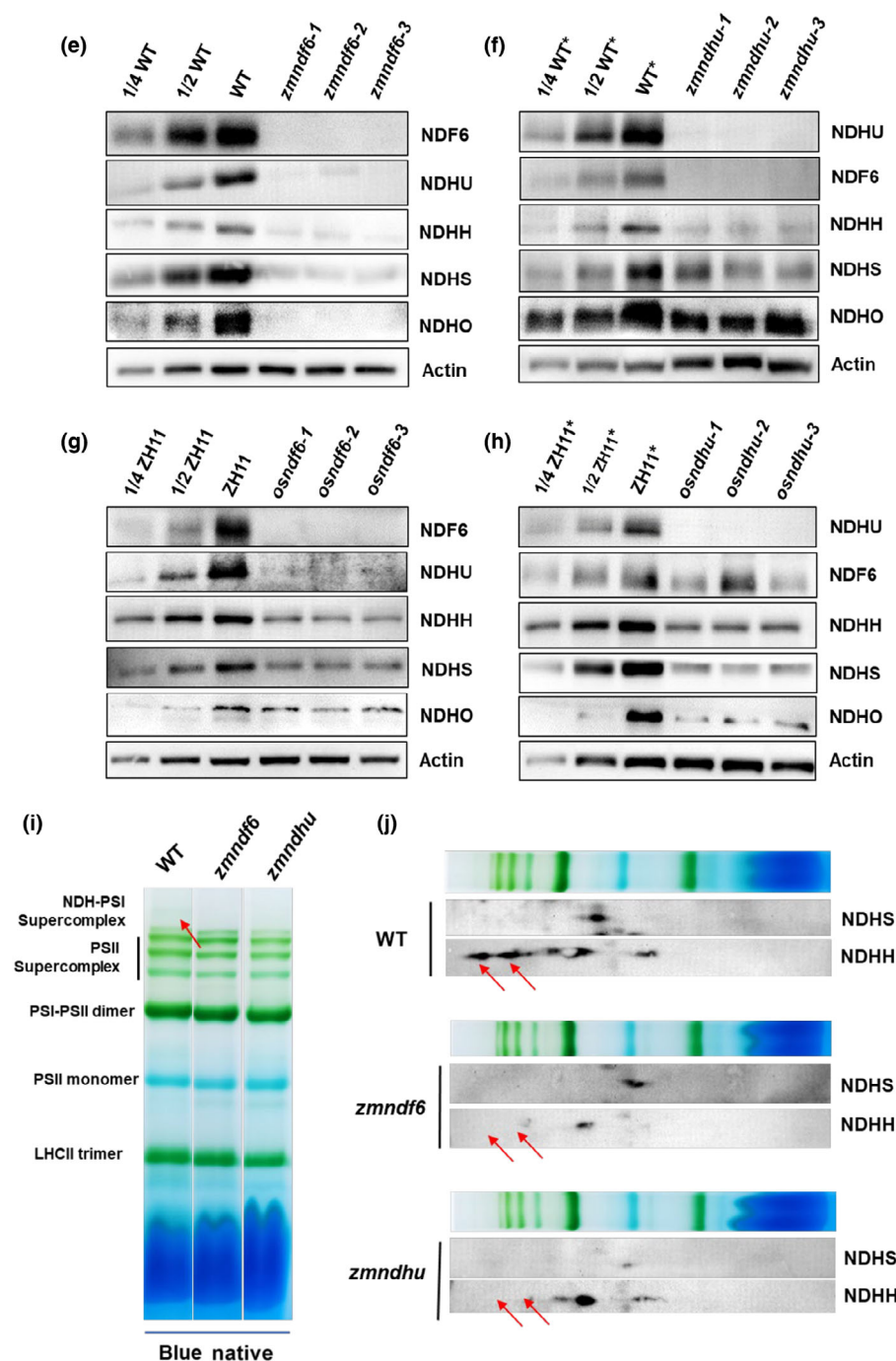
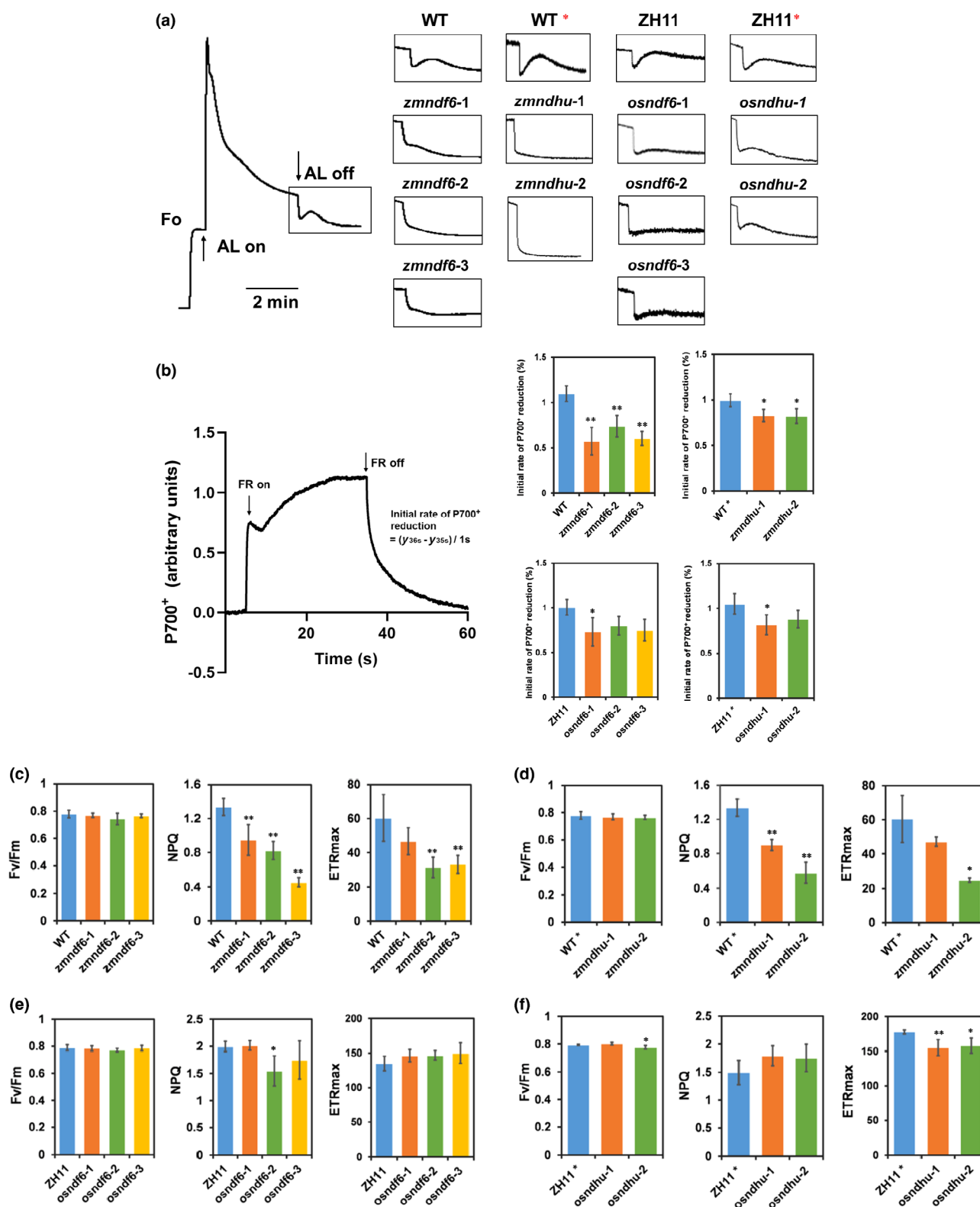


Fig. 1 (Continued).

**Fig. 2** Photosystem I (PSI) cyclic electron flow was decreased in both maize and rice *ndh* mutants but with different changes in other light reaction parameters. (a) Measurement of NDH cyclic electron transport (CET) activity, which was detected as a transient increase in Chl fluorescence (surrounded by a box) after turning off the AL. (b) The re-reduction of  $P700^+$  occurred after turning off the FR light, and comparison of the initial rates of  $P700^+$  re-reduction between WT and *ndh* mutants was calculated. Curves were normalized to the maximum  $P700$  oxidation level. Data are mean  $\pm$  SE ( $n = 4$  biological replicates). \*,  $P < 0.05$ ; \*\*,  $P < 0.01$  compared with WT according to Student's *t*-test. WT\* indicates the wild-type (WT) used in a different batch together with *zmndhu* mutants, and ZH11\* indicates the WT used in a different batch together with *osndhu* mutants, due to timing and availability of transgenic materials. (c–f) Significant decrease in photosynthetic light reaction parameters in maize but not in rice *ndh* mutants. Fv/Fm (maximal PSII quantum efficiency), NPQ (nonphotochemical quenching), and ETRmax (maximal electron transport rate) were estimated from light response curve. Data are mean  $\pm$  SE ( $n = 4$  biological replicates). \*,  $P < 0.05$ ; \*\*,  $P < 0.01$  compared with WT according to Student's *t*-test.



(Fig. 2c,d). Consistent with these observations, a decrease in steady-state photosynthetic rate and photoprotective NPQ was reported in the *ndhm* and *ndho* mutants of maize (Peterson *et al.*, 2016).

The initial slopes of the *A/C<sub>i</sub>* curve, and the level of steady-state photosynthetic rate, were not notably different from WT in the rice *osndf6* and *osndhu* mutants (except that the *A/C<sub>i</sub>* curve of *osndf6* mutants appeared lower than WT; Fig. 3c,d).

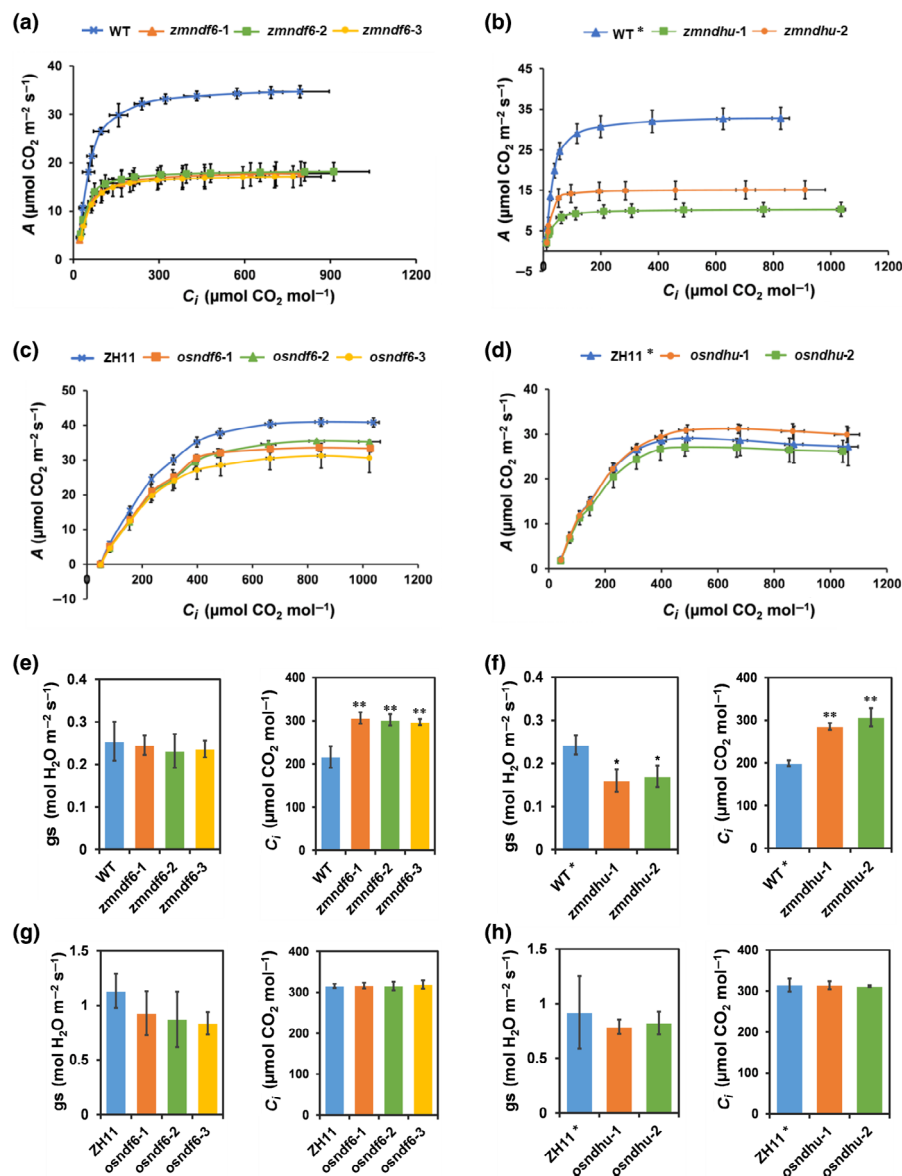


**Fig. 3** CO<sub>2</sub> assimilation was severely inhibited in maize but not in rice *ndh* mutants. (a–d) CO<sub>2</sub> response curve of net photosynthetic assimilation rate ( $A/C_i$ ) measured at 1200  $\mu\text{mol photons m}^{-2} \text{ s}^{-1}$  and 28°C ( $n = 3$  biological replicates). See Supporting Information Dataset S6 for the statistics of  $A/C_i$  curves. (e–h) Stomatal conductance (gs) and intercellular CO<sub>2</sub> concentration (C<sub>i</sub>) measured at 28°C and 400  $\mu\text{mol CO}_2 \text{ mol}^{-1}$ . Data are mean  $\pm$  SE ( $n = 3$  biological replicates). \*,  $P < 0.05$ ; \*\*,  $P < 0.01$  compared with wild-type (WT) according to Student's *t*-test. WT\* indicates the WT used in a different batch together with *osndhu* mutants, and ZH11\* indicates the WT used in a different batch together with *osndhu* mutants, due to timing and availability of transgenic materials.

Measurements of ETR and NPQ also showed no significant difference between the rice *ndh* mutants and the WT (Fig. 2e,f).

It is noteworthy that while the stomatal conductance (gs) of the *zmndf6* and *zmndhu* mutants was not different, or even lower, than that of the WT, the intercellular CO<sub>2</sub> concentration (C<sub>i</sub>) was increased (Fig. 3e,f). This implies that CO<sub>2</sub> assimilation was inhibited but that this was not due to stomatal limitation. Changes in stomatal conductance and intercellular CO<sub>2</sub> concentration in the rice *ndh* mutants were not obvious (Fig. 3g,h).

#### Abnormal chloroplast ultrastructure and ROS accumulation in maize *ndf6* and *ndhu* mutants

To explore the relationship between the amount and integrity of the NDH-PSI protein complex and thylakoid lamellar structure of maize BS chloroplasts, transmission electron microscopy was performed on maize WT and *zmndf6* leaf samples. Compared

with the WT, nonstacking stromal thylakoid tended to be less assembled in the BS chloroplasts of the maize *zmndf6* mutant, and areas with intermittent distribution or even absence of lamellae were observed (Fig. 4a,b,e,f). For M cell chloroplasts, the thickness of the grana thylakoid was decreased and the grana lamellae were not well aligned in the *zmndf6* mutant compared with the WT (Fig. 4c,d,g,h). In addition, the starch granule accumulation of BS cells was lower in the mutant than in the WT (Fig. 4a,b,e,f). In accordance with this, starch staining by I<sub>2</sub>-KI in leaf paraffin sections showed that both the amount of starch synthesized early in the day and the accumulation late in the day were lower in the *ndh* mutants than that in the WT (Fig. 4j). The decrease in starch content is probably related to the decreased photosynthetic activity in maize *ndh* mutants (Fig. 3).

One of the reasons causing the impaired chloroplast ultrastructure could be the potential photo-oxidative stress suffered by the maize *ndh* mutants, as also indicated by the decreased capacity of



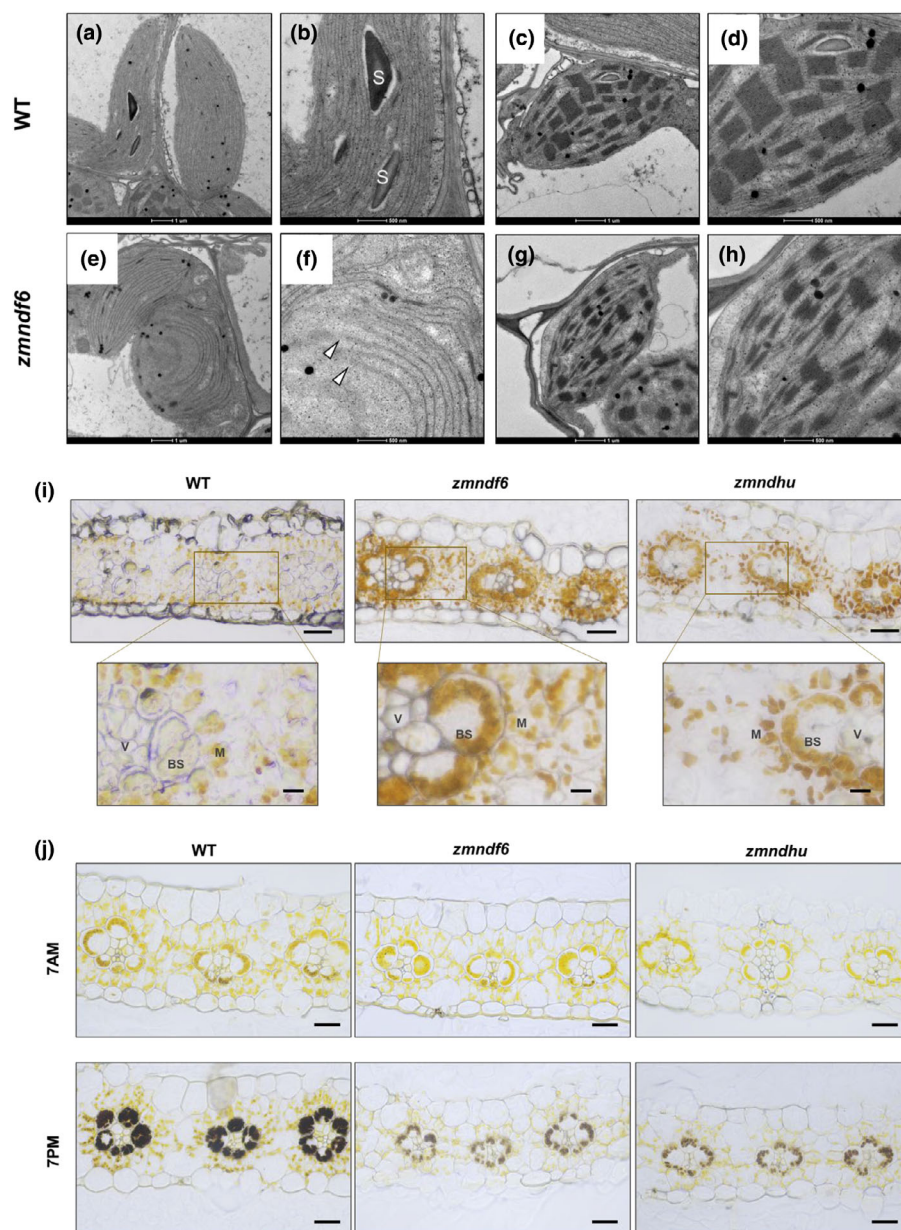


**Fig. 4** Abnormal chloroplast structure and accumulation of reactive oxygen species (ROS) and starch in maize *ndh* mutant leaves. (a–h) Abnormal thylakoid ultrastructure of bundle sheath (BS) and M chloroplasts in maize *zmndf6* mutant. Transmission electron micrographs of BS chloroplast in wild-type (WT) (a, b), M chloroplast in WT (c, d), BS chloroplast in *zmndf6* (e, f), and M chloroplast in *zmndf6* (g, h) are shown. 'S' indicates starch granule. White triangles point to the broken ends of stromal thylakoid. (i) 3,3'-diaminobenzidine (DAB) stained transections showing overproduction of ROS in the BS cells of maize *zmndf6* and *zmndhu* mutants. Brown signals were densely visible in the BS cells of *zmndf6* and *zmndhu* mutants, but not in those of the WT. Lower panel images (bars, 5 μm) are enlarged from indicated area of the upper panel images (bars, 20 μm). (j) Light micrographs of transections showing less starch granules in maize *zmndf6* and *zmndhu* mutant leaves. Accumulation of starch grains in maize leaves at 7:00 h and 19:00 h visualized by I<sub>2</sub>-KI (iodine in potassium iodide solution) staining. Bars, 20 μm.

NPQ (Fig. 2c,d). We detected the accumulation of reactive oxygen species (ROS) in the BS and M cells by 3,3-Diaminobenzidine (DAB) staining that reacts with H<sub>2</sub>O<sub>2</sub> (Fig. 4i; Thordal-Christensen *et al.*, 1997). Brown signal was densely exhibited in the BS chloroplasts of *zmndf6* and *zmndhu* mutants, and brown staining was also visible in the neighboring M chloroplasts. In the WT, overall staining intensity was much less than that in the *ndh* mutants (Fig. 4i). These results indicate an increase in ROS accumulation in both BS and M cells when NDH is deficient in maize leaves.

### Effects of NDH deficiency on the BS cell proteome

In order to further explore the effect of NDH deficiency specific in maize BS cells, we conducted a proteomic analysis by comparing the isolated BS cells of WT and the *zmndf6* mutant. First of

all, the purity of the BS preparation was assessed. As expected, Western blot analysis showed that RbcL was enriched in the BS rather than M preparation, while PPDK was found in an opposite distribution pattern (Fig. S5a). From the proteomic data, we found that contents of many NDH subunits (including NDHU, NDHM, NDHN, PnsB1, and PnsL2) significantly decreased ( $P < 0.01$ ), while contents of PGR5 and PGRL1 remained less changed, confirming that the mutation of ZmNDF6 had decreased the abundance of NDH complex in maize BS cells (Fig. 5a). The contents of BS-specific C<sub>4</sub> enzyme NADP-ME and Rubisco activase (especially RCA2) increased (Fig. 5a,b), while the contents of Rubisco subunits were not significantly changed in the tested lines (from both BS cells and whole leaves; Fig. S5b). Interestingly, fructose-bisphosphate aldolase (SFBA) content was enhanced whereas fructose-1,6-bisphosphatase (FBPase) content declined (Fig. 5a). Further analysis of the

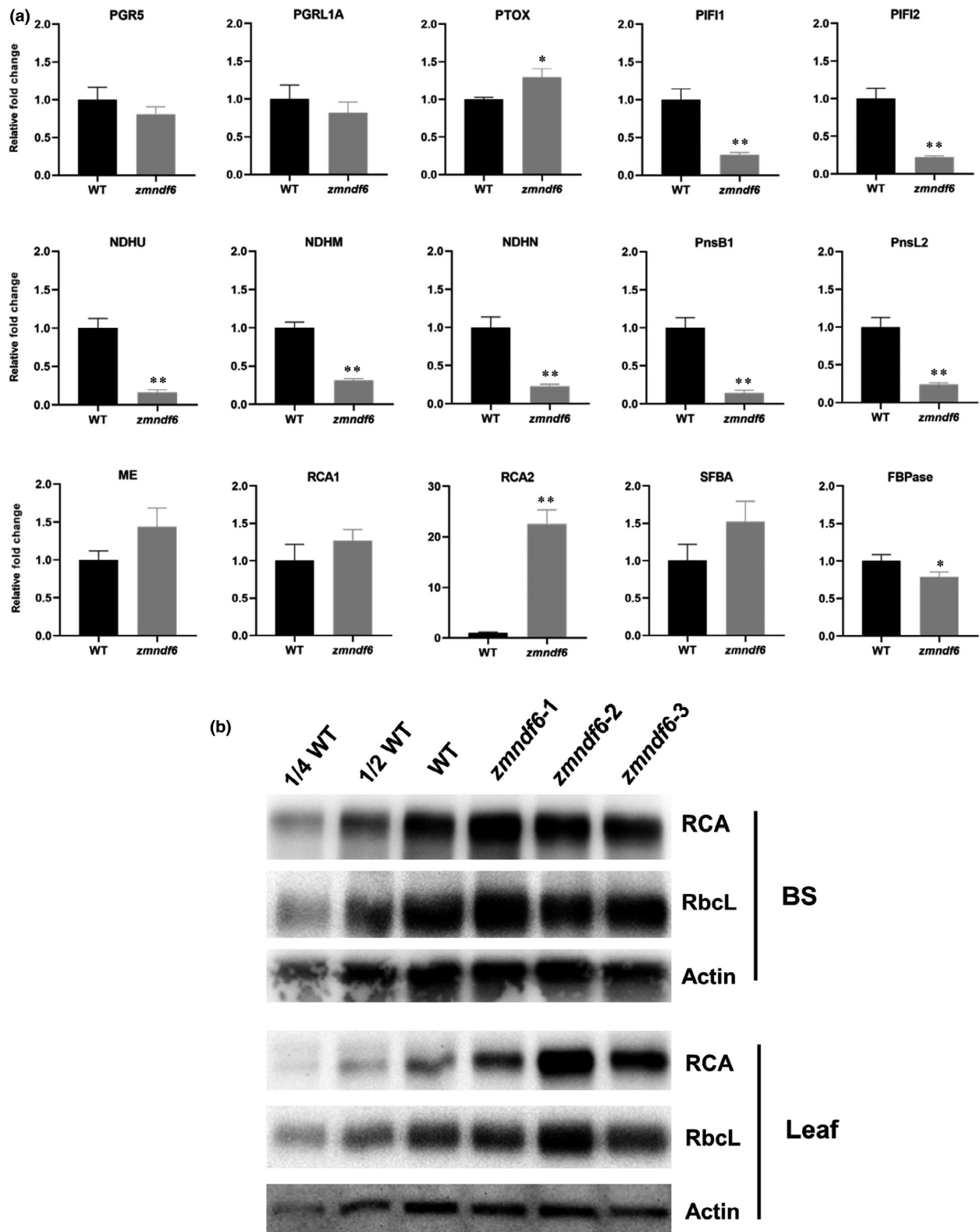


**Fig. 5** Changes in bundle sheath (BS) cell-specific cyclic electron transport (CET) pathway and CO<sub>2</sub> assimilation-related proteins. (a) Comparisons were made between maize wild-type (WT) and *zmndf6* mutant according to quantitative values from bundle sheath (BS) cell proteomics. Data are mean  $\pm$  SE ( $n = 3$  biological replicates). \*,  $P < 0.05$ ; \*\*,  $P < 0.01$  compared with WT according to Student's  $t$ -test. (b) Immunoblot analysis reveals trends of increased amount of Rubisco activase and relatively less changed amount of RbcL protein (the relative amounts between samples varied from batch to batch, but trends have been clear), in the BS cells or whole leaves of maize *ndf6* mutant compared with those in WT.

proteins involved in starch metabolism revealed that beta-amylase (BAM9), which is a nonenzymatic regulator of leaf starch degradation, was significantly upregulated ( $P < 0.05$ ; Fig. S5b; David *et al.*, 2022). This may be also related to the decreased starch content in the maize *ndh* mutants (Fig. 4j).

Moreover, proteins associated with the PSI complex were significantly less in *zmndf6* mutant ( $P < 0.01$  or  $< 0.05$ ; Fig. S5c). Since PSI and NDH form a supercomplex, the deficiency of NDH complex in the *zmndf6* mutant seems to also affect the abundance of PSI proteins. Components of ATP synthase appeared to be stable, while components related to the Cytb6/f complex (PetA, PetD, and PetC for example) decreased in *zmndf6* BS cells (Fig. S5c). It is worth noting that STN7 and STN8 (involved in state transition), as well as ferredoxin-NADP<sup>+</sup> reductase 1 (FNR1) and FNR3 (responsible for electron transport between NADPH and ferredoxin), were significantly upregulated in *zmndf6* BS cells ( $P < 0.01$ ), indicative of large changes in distribution of light energy and electron flow (Fig. S5c). Analysis of the changes in proteins related to redox regulation showed significant downregulation of thioredoxin and peroxidase ( $P < 0.01$  or  $< 0.05$ ), indicating that loss of ZmNDF6 seriously affected the redox environment in maize BS cells (Fig. S5b).

Overall, the protein abundance of NDH subunits, BS-specific C<sub>4</sub> enzymes, and PSI-associated components showed similar trends, although different sample processing and sensitivities of the methods may have caused inconsistency for certain proteins between Western blots and proteomics.

### Increased transcript abundance for genes involved in the Calvin–Benson cycle and cyclic electron transport in maize *ndh* mutants

At the transcriptional level, after RNA sequencing we systematically analyzed the differential transcript accumulation of photosynthesis-related functional genes, which were converted from a complete list of maize photosynthetic proteins provided in Friso *et al.* (2010). Generally, transcript accumulation in the two maize *ndh* mutants behaved differently from the rice *ndh* mutants, with transcript abundance linked with the CET pathway and Calvin–Benson cycle mostly higher in the maize mutants (Fig. 6, for details with gene lists see Fig. S6).

The transcript abundance of genes involved in LET (such as PSII, PSI, cytochrome b6f and ATP synthase) showed varied changes in the maize *zmndf6* and *zmndhu* mutants. The transcript abundance of genes encoding LHCII-1.4 and LHCII-1.5 was drastically and uniformly downregulated (up to 8.6-fold) in the two maize mutants. Those upregulated include genes encoding OEC23-like oxygen-evolving complex, PsbS, and Rieske domain protein (Fig. S6a,b). As for the components related to CET, the *zmndf6* and *zmndhu* mutants displayed downregulation of *NDF6* and *NDHU*, as expected, and lower transcript level of an extra gene of *NDF2*. Apart from that, the transcript abundance of *PGR5* and other NDH pathway-associated nuclear genes showed consistent trends of upregulation, including *PTOX* (plastid terminal oxidase) and *PIFI* (postillumination chlorophyll fluorescence increase; Fig. S6b). In the rice *osndf6* and *osndhu*

mutants, the transcript abundance of genes involved in LET showed consistent downregulation. Interestingly, although most transcripts related to CET were downregulated in the two rice mutants, *PTOX* and *PIFI* (involved in chloroplast respiration) were upregulated (Fig. S6a,b).

In maize *zmndf6* and *zmndhu* mutants, the transcript abundance of genes related to the Calvin–Benson cycle and photorespiration was often upregulated, especially for Rubisco activase (RCA) and fructose-bisphosphate aldolase-2 (SFBA-2). One exception is the obvious downregulation of FBPase in both maize *ndh* mutants (Fig. S6c). Correspondingly, the transcript abundance of genes related to starch biosynthesis also showed extensive upregulation (Fig. S6d). In rice *osndf6* and *osndhu* mutants, there was no consistent upregulation of Calvin–Benson cycle or photorespiration-related transcript accumulation, indeed there was a tendency for downregulation (Fig. S6c).

We validated the transcript abundance of C<sub>4</sub> enzymes in the maize *zmndf6* and *zmndhu* mutants by qRT–PCR. Consistent with the transcriptomic data, the transcript abundance of major genes (more abundant in transcripts) encoding BS cell localized ME, RbcS, and RbcL1 were upregulated in *zmndf6* mutants, by 2.27, 4.26, and 4.35-fold, respectively. In contrast, the major transcript abundance of M cell localized phosphoenolpyruvate carboxylase (PEPC), malate dehydrogenase (MDH), and pyruvate phosphate dikinase (PPDK) did not markedly change or even decrease in the *zmndf6* mutants (Fig. 6c). Similarly, an increased transcript abundance of BS-specific C<sub>4</sub> genes was observed in the *zmndhu* mutant. As chloroplast signals participate in nucleus-plastid communication (Surpin *et al.*, 2002; Baier & Dietz, 2005), the redox changes within chloroplasts caused by lack of NDH (Figs 4i, S4a) may be one of the reasons for these transcript abundance changes, and this in turn could affect the protein changes in the BS.

### Impaired NDH-CET causes critical changes in photosynthetic carbon metabolism in maize

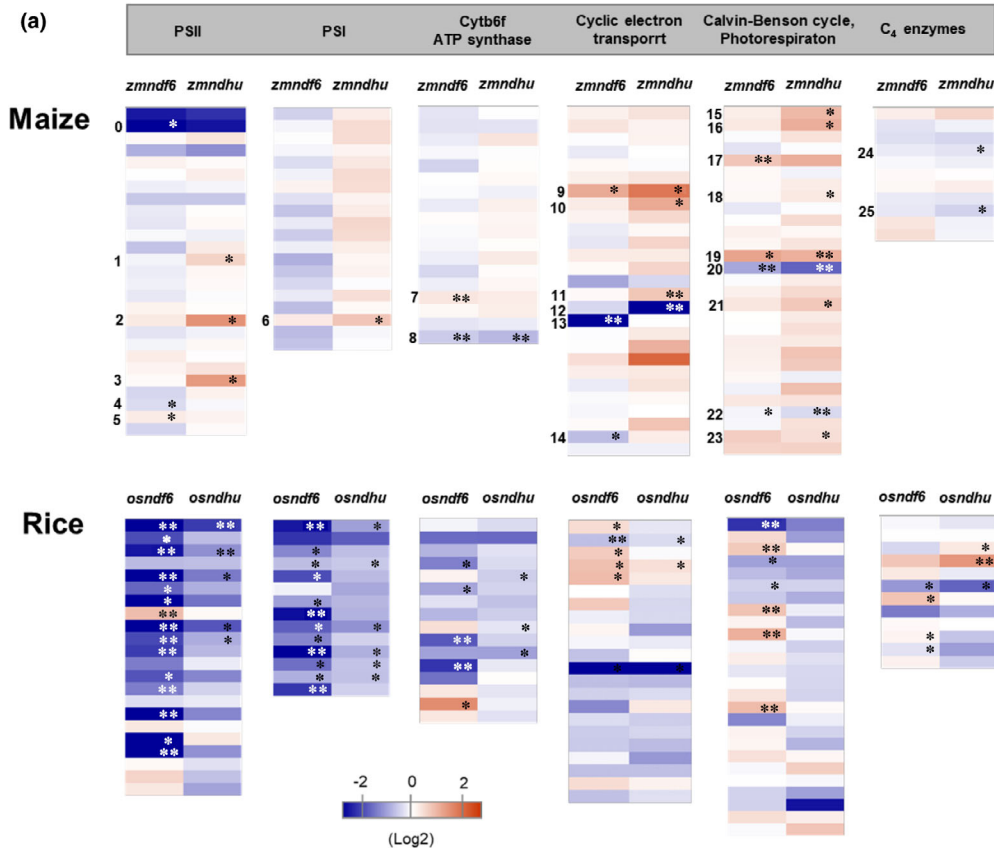
The measured changes in photosynthesis, transcript abundance, and protein contents suggested that NDH deficiency had different impacts on CO<sub>2</sub> assimilation in maize and rice. We therefore examined how NDH influenced photosynthetic metabolism using the maize and rice leaves for metabolic analysis. Metabolic profiles of the maize *zmndf6* and *zmndhu* mutants were found to be relatively consistent with each other, with obvious common upregulated or downregulated components (Fig. 7a). Specifically, metabolites involved in the Calvin–Benson cycle in maize *ndh* mutants were generally decreased compared with the WT, except for ribulose 1,5-bisphosphate (RuBP) and fructose 1,6-bisphosphate (FBP), which accumulated significantly ( $P < 0.01$  or  $< 0.05$ ; Fig. 7a,d). In contrast, metabolites at earlier steps of photorespiration increased in maize *ndh* mutants (Fig. 7a,f), indicating an increase in photorespiration, consistent with previous report in *ndhn* and *ndho* mutants of maize (Peterson *et al.*, 2016).

For the C<sub>4</sub> metabolic cycle, we found that phosphoenolpyruvate (PEP), pyruvate (Pyr), and aspartate (Asp) decreased to



varying degrees, whereas malate increased in both *zmndf6* and *zmndhu* mutants (Fig. 7a,e), which correlates with the increased transcript abundance and protein content of NADP-ME (Figs 5a, 6c). Changes in malate probably also led to the accumulation

of fumaric acid (Fum), which interconverts with it in the tricarboxylic acid cycle (TCA cycle; Fig. 7g). It should be mentioned that many of the metabolites are compartmentalized with a sub-pool being involved in C<sub>4</sub> metabolism, the case of malate being



(b)

	Name		Name
0	LHCII-1.4 and 1.5 families	13	NDH F6 (PnsB4)
1	PSII Lumen Tat ITP -1	14	CRR6
2	OEC23-like-1	15	RBCS-4-2
3	OEC23-like-6 Tat ITP TP21.5	16	RBCS-4-1
4	psbR	17	RCA
5	psbS	18	PGK-1 (M-enriched)
6	psaL	19	SFBA-2
7	Rieske [2Fe-2S] domain protein	20	FBPase
8	FNR-1	21	SBPase
9	PIFI-1	22	PGP
10	PIFI-2	23	CAT1
11	PnsB3	24	PEPC
12	NDH U	25	AspAT

(c)

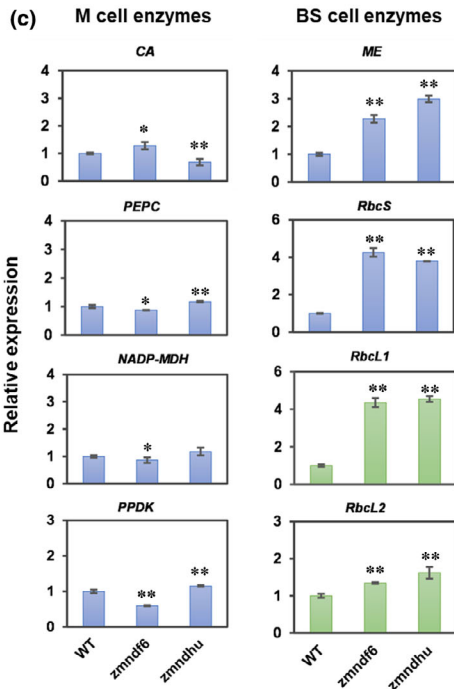




**Fig. 6** Changes in transcript abundance and bundle sheath (BS) cell protein content in maize *ndh* mutants. (a) Heatmap shows differentially accumulated transcripts in *ndh* mutants relative to their wild-types (WTs; see Supporting Information Fig. S6 for the heatmap with gene list). The significantly changed genes are assigned with numbers that link to names of encoded proteins in (b). The data represents mean value of three biological replicates. (b) Names of proteins encoded by significantly changed genes from (a). Red upward and blue downward arrows indicate the transcript level rose or fell in both mutants, even if only significant on one mutant (or those were inconsistent between two mutants, e.g. 1 and 14). (c) RT-PCR validation showing increased transcript accumulation of BS but not M-specific  $C_4$  genes in maize *ndh* mutants. CA, carbonic anhydrase; ME, malic enzyme; NADP-MDH, NADP malate dehydrogenase; PEPC, phosphoenolpyruvate carboxylase; PPK, pyruvate phosphate dikinase; RbcL1, Rubisco large subunit 1; RbcL2, Rubisco large subunit 2; RbcS, Rubisco small subunit. Data are mean  $\pm$  SE ( $n=3$  biological replicates). \*,  $P<0.05$ ; \*\*,  $P<0.01$  compared with WT according to Student's *t*-test. See Dataset S7 for the summary of primers used.

an example. It is possible that the changes observed are not only in the pool that is involved in  $C_4$  metabolism. We were not able to clarify the metabolomics in BS cells at this stage.

We calculated the ATP : ADP, NADH : NAD, and NADPH : NADP ratios, with the results indicating that the ATP : ADP ratio is similar in WT and the maize mutants, whereas the NADPH : NADP ratio is strongly increased in the two *ndh* mutants of maize ( $P<0.01$  or  $<0.05$ ; Fig. 7h). The NADPH : NADP ratio is important because several of the reactions in which NADPH is involved are reversible.

The metabolic profiles of rice *osndf6* and *osndhu* mutants displayed more variable fluctuations (variable between replicate lines, and between the two mutants, for a given metabolite), but with an overall trend of decreased contents (Fig. 7b,c). On the contrary, while the levels of adenylates and NADPH in maize *ndh* mutants increased, the levels in the rice *ndh* mutants appeared to decrease or showed no consistent change (Fig. 7b,c).

## Discussion

To maintain an efficient Calvin–Benson cycle in the framework of the  $C_4$  pathway, it is necessary to dynamically balance the metabolism of both substance and energy. In this study, we show that NDH-mediated CET plays a crucial role in this process. The necessity and continuity of this regulation may be more prominent in driving the Calvin–Benson cycle in the  $C_4$  BS cells of maize. Fig. 8 provides a summarized interpretation.

This has been investigated using maize and rice loss-of-function mutants of NDF6 and NDHU subunits generated by CRISPR–Cas9 technology. In the leaves of our homozygous lines of *ndh* mutants in maize and rice, the protein amounts of NDF6, NDHU as well as some of other NDH subunits, were greatly decreased. A similar trend was found in the BS cells of the maize *ndf6* mutant. NDF6 and NDHU were chosen not only because of their higher expression in maize than in rice (Fig. S1) but also because of their higher BS : M distribution ratio, for both mRNA and protein (Table S1).

NDF6 (also known as PnsB4) is an integral part and a *trans*-membrane subunit of the NDH complex, which may be crucial for maintaining the stability of NDH, and NDHU is a chloroplast-specific subunit located close to the electron donor Fd binding site (Shen *et al.*, 2022; Su *et al.*, 2022). Although NDF6 and NDHU may have specific functions independent of a primary role in NDH, the similar changes in growth phenotype, photosynthetic parameters, and metabolites in our maize *ndf6* and *ndhu* mutants provide new opportunities to explore the roles of NDH in a  $C_4$  plant.

## NDH cyclic electron transport balances $C_4$ metabolism and carbon flow

Using NDH-deficient mutants of maize and rice for comparison, we found that the metabolite and energy flows were effectively disrupted for  $C_4$  but not for  $C_3$  photosynthesis. It is known that the direct electron donor of NDH is ferredoxin (Fd), and electrons can be transferred between NADPH and Fd through ferredoxin–NADP<sup>+</sup> reductase (FNR; Ifuku *et al.*, 2011; Peltier *et al.*, 2016; Iyanagi, 2022). Since NADPH generation is coupled to decarboxylation of the malate entering into BS cells, NDH may play a special role in maintaining the electron flow of PSI, regeneration of NADP<sup>+</sup>, and the continuous input of malate along the concentration gradient. This study demonstrates that both NADPH and malate tend to accumulate in maize *zmndf6* and *zmndhu* mutants, which is different from the situation in equivalent mutants in rice (Fig. 7). The accumulation of malate and NADPH could be caused by the impaired NADPH turnover and exacerbated by the decreased demand from Calvin–Benson cycle, as reflected by the accumulation of RuBP and lower levels of many other intermediates (Fig. 7) in maize *ndh* mutants. In contrast, photorespiration was favored, leading to more production of 2-phosphoglycolate, and elevated levels of other intermediates in the first part of the pathway, such as glycolate and glyoxylate. This provides metabolic support for the increased photorespiration in maize *ndhn* and *ndho* mutants proposed by Peterson *et al.* (2016). This earlier work used gas exchange measurements of the oxygen sensitivity of photosynthesis in combination with modeling, to show that photorespiration was increased, predicting a decrease in CO<sub>2</sub> level in the BS.

It is worth noting that the distinct decrease in transcript abundance for FBPase, together with the increase in transcript abundance for SFBA, echoes well with the FBP accumulation in maize *ndh* mutants (Fig. S6c), indicating an important site-specific regulation which is pending to be resolved. The accumulation of FBP also indicated an effect of the NDH pathway on rate-limiting steps of the Calvin–Benson cycle, and its involvement in the feedback regulation of CET, as the FBPase-deficient mutant (*hcefl*) was reported to specifically upregulate NDH and increase CEF (Livingston *et al.*, 2010a,b). In addition, we speculate that the decreased CO<sub>2</sub> level and ATP supply in BS cells of NDH-deficient mutants are responsible for the concomitant decrease in carboxylation rate and increase in RuBP levels observed. If Rubisco protein abundance is less changed, there might be more pressure for Rubisco activase to change to compensate; thus, the feedback upregulation of its transcripts and protein abundance becomes reasonable (Figs 5, 6).



**Fig. 7** Loss of NDH-CET in maize leads to disturbance of key photosynthetic metabolites. (a) Relative abundance ( $\log_2$ -transformed fold changes) of photosynthetic metabolites in maize *zmndf6* and *zmndhu* mutants. WT: The mean of  $\log_2$ -fold changes in four WT (KN5585) values relative to their average. S1–S4: Fold changes in mutant values relative to the average value of WT. \*,  $P < 0.05$ ; \*\*,  $P < 0.01$  compared with WT according to Student's *t*-test. (b, c) Relative abundance ( $\log_2$ -transformed fold changes) of photosynthetic metabolites in rice *osndf6* and *osndhu* mutants. ZH11, the mean of  $\log_2$ -fold changes of six WT (ZH11) values relative to their average; S1–S6, fold changes in mutant values relative to the average value of WT. \*,  $P < 0.05$ ; \*\*,  $P < 0.01$  compared with WT according to Student's *t*-test. (d–g) Schematic diagrams showing key metabolites in (d) Calvin–Benson cycle (Berg *et al.*, 2007), (e)  $C_4$  metabolic cycle (the dotted arrows pointing from PEP through OAA to Asp indicate the likely reduced activity of this pathway in the *ndh* mutants), (f) photorespiration pathway, and (g) EMP, PPP pathways, and TCA cycle of maize *ndh* mutants. Heatmap arrays derived from *zmndf6* (upper row) and *zmndhu* (lower row) are listed on the side of corresponding metabolites. EMP pathway, Embden–Meyerhof–Parnas pathway, also known as glycolysis. PPP pathway, pentose phosphate pathway. TCA cycle, tricarboxylic acid cycle. (h) Ratios of NADPH : NADP, NADH : NAD, and ATP : ADP. Data are mean  $\pm$  SE ( $n = 4$  biological replicates). \*,  $P < 0.05$ ; \*\*,  $P < 0.01$  compared with WT according to Student's *t*-test. Metabolite names showed in this figure are as follows: 2PG, phosphoglyceric acid; ADP, adenosine diphosphate; ADPG, adenosine diphosphate glucose; aKG,  $\alpha$ -ketoglutaric acid; Ala, alanine; Asp, aspartate; ATP, adenosine triphosphate; CIT, citric acid; DPGA, 1,3-bisphosphoglyceric acid; E4P, erythrose 4-phosphate; F6P, fructose 6-phosphate; FBP, fructose 1,6-bisphosphate; Fum, fumaric acid; G6P/G1P, glucose 6-phosphate/glucose 1-phosphate; GAP/DHAP, 3-phosphoglyceric acid/dihydroxyacetone; Gln, glutamine; Glu, glutamate; Glx, glyoxylic acid; Gly, glycine; Glyce, glyceric acid; Glyco, glycolic acid; Hpyr, hydroxypyruvic acid; ICIT, isocitric acid; Mal, malic acid; NAD, nicotinamide adenine dinucleotide; NADH, nicotinamide adenine dinucleotide reduced; NADP, nicotinamide adenine dinucleotide phosphate; NADPH, nicotinamide adenine dinucleotide phosphate reduced; OAA, oxaloacetic acid; PenP, pentose phosphate, mix of ribose 5-phosphate, xylulose 5-phosphate and ribulose 5-phosphate; PEP, phosphoenol pyruvate; PGA, 3-phosphoglyceric acid; Pyr, pyruvate; RuBP, ribulose 1,5-bisphosphate; S7P, sedoheptulose 7-phosphate; Ser, serine; Succ, succinic acid; UDPG, uracil-diphosphate glucose.

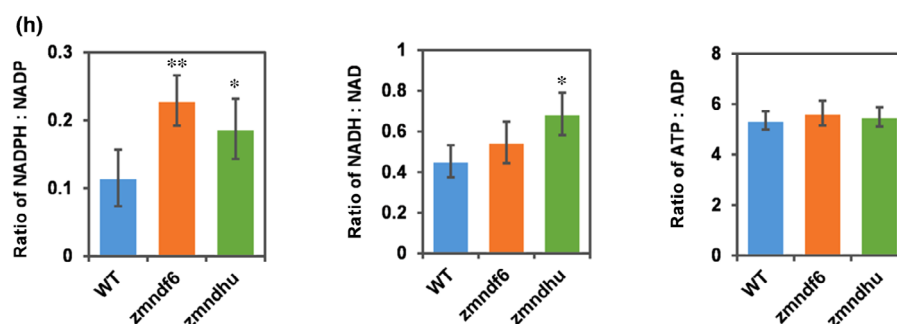


**Fig. 7** (Continued).

chloroplasts have little PSII, disruption of NDH-CET may interfere with the provision of electrons for the reduction of ferredoxin and hence thioredoxin, thus negatively affecting the activation of target enzymes. On another hand, the accumulation of malate and NADPH in *zmndhu* mutants is probably responsible for the over-reduced state of chloroplast stroma and the obstructed status of electron transport chain (Figs 2c–f, S4a). The increased ROS accumulation in the BS cells of *zmndf6* and *zmndhu* mutants (Fig. 4i) would be caused by this over-reduction, and this could negatively affect the photosynthetic proteins, photosynthetic rate, and plant growth (Figs 1, 3, S4b,c).

The decarboxylation of  $C_4$  acids in the BS cells is a key step in  $C_4$  photosynthesis. Maintaining a suitable oxidized status in BS cell chloroplasts is proposed to be required for efficient  $C_4$  photosynthesis (Zhao *et al.*, 2022). NADP-ME operation in the direction of decarboxylation is known to be hampered by a high NADPH : NADP ratio, as recently highlighted by Bräutigam *et al.* (2018), indicating that oxidized redox poise in the chloroplast stroma favors high velocity of decarboxylation. They proposed that BS chloroplasts achieve a more oxidized state via the consumption of NADPH by Calvin–Benson cycle and the limited production of NADPH by abolishing PSII activity in BS cells. Here, our results suggest a third driving force, which is NADPH turnover by BS-enriched NDH-CET. In maize BS

cells, where malate is imported and decarboxylated to release NADPH, the loss of NDH-CET could lead to the observed increase in NADPH levels and NADPH : NADP ratio, which in turn restricts decarboxylation by NADP-ME, leading to lower BS  $CO_2$  concentration, lower pyruvate content, and overaccumulation of malate. Lower BS  $CO_2$  would restrict the Rubisco carboxylase reaction providing a potential explanation for the higher RuBP. This would increase the Rubisco oxygenase reaction, providing a potential explanation for the observed higher levels of intermediates in the first part of the photorespiration pathway. In agreement, Peterson *et al.* (2016) suggested that impaired capacity to generate ATP in the BS of NDH-deficient maize is associated with depressed processing of malate by NADP-ME due to restricted utilization of the product NADPH. This results in slower turnover of the  $C_4$  cycle and decreased concentration of  $CO_2$  around Rubisco.

As part of the early attempts to install the  $C_4$  pathway,  $C_4$ -specific NADP-ME was overexpressed in rice, but it led to bleaching of leaf color and growth hindrance, which resulted from enhanced photoinhibition due to an increase in the level of NADPH inside the chloroplast (Tsuchida *et al.*, 2001). The malate and NADPH imbalance, pale green leaf, retarded growth, and ROS accumulation observed in our maize NDH-deficient mutants are reminiscent of the effect of NADP-ME

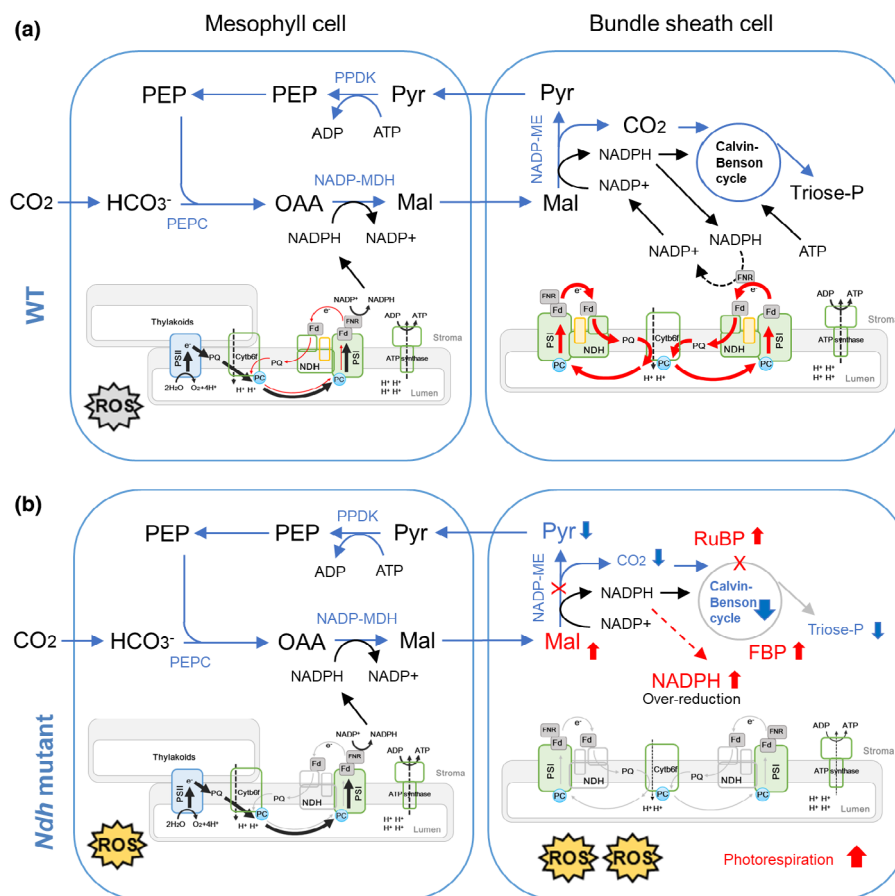


**Fig. 8** Schematic summary of the significance of NDH-mediated cyclic electron transport (CET) in maize  $C_4$  photosynthesis. (a) In the BS cells of wild-type (WT) maize, malate is imported from M cells and mainly decarboxylated by NADP-ME, to release  $CO_2$  and at the same time generate NADPH.  $CO_2$  and NADPH are used in the Calvin-Benson cycle. Some of the NADPH may be involved in maintaining PSI-CET (which drives ATP production) through the enriched NDH complex (bold red arrows compared with the thin red arrows in M cells), thus forming electron flows from malate to NADPH, from NADPH to PQ (via FNR, Fd, and NDH), and from PQ to PSI (through PC) or  $H_2O$  (through PTOX), as there is almost no PSII-LET in the BS cells. Maize BS cells have low levels of PSII, but we are not showing BS PSII in this diagram to save place and emphasize the enrichment of PSI; the electron flow from NADPH via FNR to Fd is reversible, while we have made the arrow single way for easier understanding; NDF6 (PnsB4) belongs to subcomplex B in orange color. It should be noted that 3PGA/triose-P shuttle is also important for delivery of ATP and NADPH to the BS cells, but is not presented due to tight schematic layout. ROS generation preferentially occurs in the M cells. (b) For a general comparison with WT, in the BS cells of maize *ndh* mutants, PSI-CET is inhibited (thin gray arrows), with malate and NADPH accumulating (colored red), leading to redox imbalance, decreased  $CO_2$  fixation (colored blue), increased ROS accumulation, and increased photorespiration. Calvin-Benson cycle was inhibited in maize *ndh* mutants as reflected by the decrease in many metabolites but specific accumulation of RuBP and FBP. In addition, as combined effects of malate import and NDH deficiency, BS cells of maize *ndh* mutants suffered from an over-reduced condition. The altered redox status and metabolite flow may disturb the cellular environment and cast effects on transcript and protein accumulation patterns.

overexpression. The NDH deficiency-related redox imbalance specific to maize BS cells could be responsible for the increased ROS level even under normal light. It should be noted that potential changes in ATP availability for the Calvin-Benson cycle in the BS cells of maize *ndh* mutants could also lead to multiple consequences. Therefore, a functional or enhanced operation of NDH-CET may be a prerequisite when considering reconstruction of the  $C_4$  cycle.

### Deficiency of NDH disrupts the coordination of transcript and protein accumulation in $C_4$ plants

The compartmentalization of photosystems and  $C_4$  enzymes between BS and M cells is essential for the operation of  $C_4$  photosynthesis in maize. The regulatory mechanisms behind

$C_4$  differentiation remain unclear, but they probably involve the coordination of nuclear and plastid genomes, or specific changes in the intracellular environment to control gene expression in  $C_4$  leaves. Because of the abundance of the NDH complex in maize BS cells, and its important role discussed previously, our maize *zmndf6* and *zmndhu* mutants can be viewed as having cellular changes mainly in the BS. In particular, changes in the redox state of PQ pools in the chloroplast can affect nuclear gene expression through retrograde signal transduction (Foyer *et al.*, 2012). Our data showed that the transcript abundance of the BS cell-specific  $C_4$  enzymes ME, RbcS, and RbcL1 were increased significantly, whereas the transcript abundance of M cell-specific enzymes PEPC, MDH, and PDK did not change or decrease in *zmndf6* mutants (Fig. 6c). The BS-specific protein contents of NADP-ME and Rubisco activase were



consistently increased, but we were unable to confirm changes for Rubisco subunits, which might be subject to more regulation or change on protein level.

Interestingly, according to the transcriptome analysis, apart from the CRISPR-targeted *NDF6* and *NDHU* genes, the transcript abundance of many other NDH pathway-associated nuclear genes, as well as *PGR5* and *PTOX*, showed various degrees of upregulation (Fig. S6b) in the maize *zmndf6* and *zmndhu* mutants. One possible trigger could be the increased ROS accumulation in these mutants, as Strand *et al.* (2015) found that treatment of leaves with H<sub>2</sub>O<sub>2</sub> could improve NDH complex-dependent CET activity. Equally noteworthy, Calvin–Benson cycle-related transcript abundance was often consistently increased in the two maize *ndh* mutants (Fig. S6c). We suspect that these parallel changes in transcript abundance between CET and the Calvin–Benson cycle could be a projection of the intrinsic involvement of the NDH pathway in the regulation of C<sub>4</sub> carbon metabolism.

In conclusion, as modeled in Fig. 8, NDH CET is important for the optimization of C<sub>4</sub> photosynthesis in the NADP-ME subtype species of maize. The significance of the NDH pathway in C<sub>4</sub> plants can be attributed to both ATP supply and NADPH turnover, as well as the adjustment of malate flux and NADP-ME activity. The loss of NDH function leads to metabolic, redox, and other regulatory imbalances, especially in BS cells, which then feedback to affect the coordination of photosynthetic transcript accumulation and protein levels. Our study advances the functional understanding of NDH enrichment in maize BS cells, provides support for the involvement of NDH-CET in the optimization events during C<sub>4</sub> evolution, and hopefully will inspire fine-tuning strategies to be reconsidered with the goal of engineering C<sub>4</sub> photosynthesis.

## Acknowledgements

We thank Prof. Hualing Mi and Prof. Jane Langdale for critical comments on this work. We thank You Zhang and Luhuan Ye for helping with gas exchange, chlorophyll fluorescence, and P700 measurements; Zai Shi, Rui Zhang, and Yanfei Fan for other material and instrument assistance. We are grateful to Xiaoyan Gao, Zhiping Zhang, Jiqin Li, Wenli Hu, Shanshan Wang, and Xiaoyan Xu for technical support on TEM and HPLC-MS; Chunguang Chen from ORIZYMES for antibody generation and Mi laboratory for gift of other antibodies; and WIMI Biotechnology for maize and rice mutant generation. This research was funded by the National Natural Science Foundation of China (no. 31970257), Strategic Priority Research Program (no. XDA24010203-2), and a joint grant for international exchange from the Royal Society and National Natural Science Foundation of China to Andrew J. Fleming and Peng Wang (nos. 32011530166 and IEC\NSFC\191365).

## Competing interests

None declared.

## Author contributions

QZ and PW conceived the project; QZ performed most experiments and data analyses and produced the figures; ST analyzed the RNA-seq data; QT and GC provided essential help for metabolite measurement. QZ, YZ, AJF, X-GZ and PW interpreted the results, wrote and revised the paper with input from all authors.

## ORCID

Andrew J. Fleming  <https://orcid.org/0000-0002-9703-0745>

Peng Wang  <https://orcid.org/0000-0001-5632-3130>

Yijing Zhang  <https://orcid.org/0000-0001-9568-9389>

Xin-Guang Zhu  <https://orcid.org/0000-0002-4435-130X>

## Data availability

The mRNA-seq datasets generated in this study have been deposited into the SRA database at NCBI under BioProject IDs PRJNA843342. Accession nos. for the genes measured by qRT-PCR are as follows: *ZmCA* (Zm00001eb037940), *ZmPEPC* (Zm00001eb383680), *ZmNADP-MDH* (Zm00001eb038930), *ZmPPDK* (Zm00001eb287770), *ZmME* (Zm00001eb121470), *ZmRbcS* (Zm00001eb197410), *ZmRbcL1* (Zm00001eb440790), *ZmRbcL2* (Zm00001eb187470), and *ZmEF1α* (Hughes & Langdale, 2020). Except for the antibodies of PsdD (AS09 461; Agrisera, Sweden), AtpB (AS05 085; Agrisera, Sweden), and Actin (LF208; YiChen, Shanghai), all other antibodies were made by Chunguang Chen from ORIZYMES.

## References

- Alvarez CE, Detarsio E, Moreno S, Andreo CS, Drincovich MF. 2012. Functional characterization of residues involved in redox modulation of maize photosynthetic NADP-malic enzyme activity. *Plant & Cell Physiology* 53: 1144–1153.
- Asada K, Heber U, Schreiber U. 1992. Pool size of electrons that can be donated to P700<sup>+</sup>, as determined in intact leaves: donation to P700<sup>+</sup> from stromal components via the intersystem chain. *Plant & Cell Physiology* 33: 927–932.
- Asada K, Heber U, Schreiber U. 1993. Electron flow to the intersystem chain from stromal components and cyclic electron flow in maize chloroplasts, as detected in intact leaves by monitoring redox change of P700 and chlorophyll fluorescence. *Plant & Cell Physiology* 34: 39–50.
- Baier M, Dietz KJ. 2005. Chloroplasts as source and target of cellular redox regulation: a discussion on chloroplast redox signals in the context of plant physiology. *Journal of Experimental Botany* 56: 1449–1462.
- Bauwe H, Hagemann M, Fernie AR. 2010. Photorespiration: players, partners and origin. *Trends in Plant Science* 15: 330–336.
- Berg JM, Tymoczko JL, Stryer L. 2007. *Biochemistry*, 6<sup>th</sup> edn. New York, NY, USA: W. H. Freeman and Company.
- Bräutigam A, Kajala K, Wullenweber J, Sommer M, Gagneul D, Weber KL, Carr KM, Gowik U, Mass J, Lercher MJ *et al.* 2011. An mRNA blueprint for C<sub>4</sub> photosynthesis derived from comparative transcriptomics of closely related C<sub>3</sub> and C<sub>4</sub> species. *Plant Physiology* 155: 142–156.
- Bräutigam A, Schlüter U, Lundgren MR, Flachbart S, Ebenhöf O, Schönknecht G, Christin PA, Bleuler S, Droz JM, Osborne CP *et al.* 2018. Biochemical mechanisms driving rapid fluxes in C<sub>4</sub> photosynthesis. *BioRxiv*. doi: 10.1101/387431.
- Buchanan BB. 1991. Regulation of CO<sub>2</sub> assimilation in oxygenic photosynthesis: the ferredoxin/thioredoxin system. Perspective on its discovery, present status, and future development. *Archives of Biochemistry and Biophysics* 288: 1–9.

- Burrows PA, Sazanov LA, Svab Z, Maliga P, Nixon PJ. 1998. Identification of a functional respiratory complex in chloroplasts through analysis of tobacco mutants containing disrupted plastid *ndh* genes. *EMBO Journal* 17: 868–876.
- von Caemmerer S, Ghanoum O, Furbank RT. 2017. C<sub>4</sub> photosynthesis: 50 years of discovery and innovation. *Journal of Experimental Botany* 68: 97–102.
- Chang YM, Liu WY, Shih AC, Shen MN, Lu CH, Lu MY, Yang HW, Wang TY, Chen SC, Chen SM *et al.* 2012. Characterizing regulatory and functional differentiation between maize mesophyll and bundle sheath cells by transcriptomic analysis. *Plant Physiology* 160: 165–177.
- Darje CC, Biniossek ML, Winter V, Mutschler B, Haehnel W. 2005. Isolation and structural characterization of the Ndh complex from mesophyll and bundle sheath chloroplasts of *Zea mays*. *The FEBS Journal* 272: 2705–2716.
- Darje CC, De Pascalis L, Mutschler B, Haehnel W. 2006. Studies of the Ndh complex and photosystem II from mesophyll and bundle sheath chloroplasts of the C<sub>4</sub>-type plant *Zea mays*. *Journal of Plant Physiology* 163: 800–808.
- David LC, Lee SK, Bruderer E, Abt MR, Fischer-Stettler M, Tschopp MA, Solhaug EM, Sanchez K, Zeeman SC. 2022. BETA-AMYLASE9 is a plastidial nonenzymatic regulator of leaf starch degradation. *Plant Physiology* 188: 191–207.
- Drincovich MF, Casati P, Andreo CS. 2001. NADP-malic enzyme from plants: a ubiquitous enzyme involved in different metabolic pathways. *FEBS Letters* 490: 1–6.
- Endo T, Shikanai T, Takabayashi A, Asada K, Sato F. 1999. The role of chloroplastic NAD(P)H dehydrogenase in photoprotection. *FEBS Letters* 457: 5–8.
- Ermakova M, Danila FR, Furbank RT, von Caemmerer S. 2020. On the road to C<sub>4</sub> rice: advances and perspectives. *The Plant Journal* 101: 940–950.
- Foyer CH, Neukermans J, Queval G, Noctor G, Harbinson J. 2012. Photosynthetic control of electron transport and the regulation of gene expression. *Journal of Experimental Botany* 63: 1637–1661.
- Friso G, Majeran W, Huang M, Sun Q, van Wijk KJ. 2010. Reconstruction of metabolic pathways, protein expression, and homeostasis machineries across maize bundle sheath and mesophyll chloroplasts: large-scale quantitative proteomics using the first maize genome assembly. *Plant Physiology* 152: 1219–1250.
- Furbank RT. 2017. Walking the C<sub>4</sub> pathway: past, present, and future. *Journal of Experimental Botany* 68: 4057–4066.
- Geigenberger P, Thormählen I, Daloso DM, Fernie AR. 2017. The unprecedented versatility of the plant thioredoxin system. *Trends in Plant Science* 22: 249–262.
- Horváth EM, Peter SO, Joët T, Rumeau D, Cournac L, Horváth GV, Kavanagh TA, Schäfer C, Peltier G, Medgyesy P. 2000. Targeted inactivation of the plastid *ndhB* gene in tobacco results in an enhanced sensitivity of photosynthesis to moderate stomatal closure. *Plant Physiology* 123: 1337–1350.
- Hughes TE, Langdale JA. 2020. SCARECROW gene function is required for photosynthetic development in maize. *Plant Direct* 4: e00264.
- Ifuku K, Endo T, Shikanai T, Aro EM. 2011. Structure of the chloroplast NADH dehydrogenase-like complex: nomenclature for nuclear-encoded subunits. *Plant & Cell Physiology* 52: 1560–1568.
- Ishikawa N, Endo T, Sato F. 2008. Electron transport activities of *Arabidopsis thaliana* mutants with impaired chloroplastic NAD(P)H dehydrogenase. *Journal of Plant Research* 121: 521–526.
- Ishikawa N, Takabayashi A, Noguchi K, Tazoe Y, Yamamoto H, von Caemmerer S, Sato F, Endo T. 2016a. NDH-mediated cyclic electron flow around photosystem I is crucial for C<sub>4</sub> photosynthesis. *Plant & Cell Physiology* 57: 2020–2028.
- Ishikawa N, Takabayashi A, Sato F, Endo T. 2016b. Accumulation of the components of cyclic electron flow around photosystem I in C<sub>4</sub> plants, with respect to the requirements for ATP. *Photosynthesis Research* 129: 261–277.
- Iyanagi T. 2022. Roles of ferredoxin-NADP<sup>+</sup> oxidoreductase and flavodoxin in NAD(P)H-dependent electron transfer systems. *Antioxidants* 11: 2143.
- Johnson GN. 2011. Physiology of PSI cyclic electron transport in higher plants. *Biochimica et Biophysica Acta* 1807: 384–389.
- Kouřil R, Strouhal O, Nosek L, Lenobel R, Chramrád I, Boekema EJ, Šebela M, Ilík P. 2014. Structural characterization of a plant photosystem I and NAD(P)H dehydrogenase supercomplex. *The Plant Journal* 77: 568–576.
- Kubicki A, Funk E, Westhoff P, Steinmüller K. 1996. Differential expression of plastome-encoded *ndh* genes in mesophyll and bundle-sheath chloroplasts of the C<sub>4</sub> plant *Sorghum bicolor* indicates that the complex I-homologous NAD(P)H-plastoquinone oxidoreductase is involved in cyclic electron transport. *Planta* 199: 276–281.
- Li P, Ponnala L, Gandotra N, Wang L, Si Y, Tausta SL, Kebrom TH, Provart N, Patel R, Myers CR *et al.* 2010. The developmental dynamics of the maize leaf transcriptome. *Nature Genetics* 42: 1060–1067.
- Li X, Wang P, Li J, Wei S, Yan Y, Yang J, Zhao M, Langdale JA, Zhou W. 2020. Maize GOLDEN2-LIKE genes enhance biomass and grain yields in rice by improving photosynthesis and reducing photoinhibition. *Communications Biology* 3: 151.
- Li XG, Duan W, Meng QW, Zou Q, Zhao SJ. 2004. The function of chloroplastic NAD(P)H dehydrogenase in tobacco during chilling stress under low irradiance. *Plant & Cell Physiology* 45: 103–108.
- Livingston AK, Cruz JA, Kohzuma K, Dhingra A, Kramer DM. 2010a. An Arabidopsis mutant with high cyclic electron flow around photosystem I (*hceff*) involving the NADPH dehydrogenase complex. *Plant Cell* 22: 221–233.
- Livingston AK, Kanazawa A, Cruz JA, Kramer DM. 2010b. Regulation of cyclic electron flow in C<sub>3</sub> plants: differential effects of limiting photosynthesis at ribulose-1,5-bisphosphate carboxylase/oxygenase and glyceraldehyde-3-phosphate dehydrogenase. *Plant, Cell & Environment* 33: 1779–1788.
- Ma M, Liu Y, Bai C, Yong JWH. 2021. The significance of chloroplast NAD(P)H dehydrogenase complex and its dependent cyclic electron transport in photosynthesis. *Frontiers in Plant Science* 12: 661863.
- Majeran W, van Wijk KJ. 2009. Cell-type-specific differentiation of chloroplasts in C<sub>4</sub> plants. *Trends in Plant Science* 14: 100–109.
- Majeran W, Zybailov B, Ytterberg AJ, Dunsmore J, Sun Q, van Wijk KJ. 2008. Consequences of C<sub>4</sub> differentiation for chloroplast membrane proteomes in maize mesophyll and bundle sheath cells. *Molecular & Cellular Proteomics* 7: 1609–1638.
- Mano J, Miyake C, Schreiber U, Asada K. 1995. Photoactivation of the electron flow from NADPH to plastoquinone in spinach chloroplasts. *Plant & Cell Physiology* 36: 1589–1598.
- Maxwell PC, Biggins J. 1976. Role of cyclic electron transport in photosynthesis as measured by the photoinduced turnover of P700 *in vivo*. *Biochemistry* 15: 3975–3981.
- Mi H, Endo T, Asada K. 1992. Donation of electrons to the intersystem chain in the cyanobacterium *Synechococcus* sp. PCC7002 as determined by the reduction of P700<sup>+</sup>. *Plant & Cell Physiology* 33: 1099–1105.
- Mi H, Endo T, Ogawa T, Asada K. 1995. Thylakoid membrane-bound, NADPH-specific pyridine nucleotide dehydrogenase complex mediates cyclic electron transport in the cyanobacterium *Synechocystis* PCC6803. *Plant & Cell Physiology* 36: 661–668.
- Michelet L, Zaffagnini M, Morisse S, Spalla F, Pérez-Pérez ME, Francia F, Danon A, Marchand CH, Fermani S, Trost P *et al.* 2013. Redox regulation of the Calvin–Benson cycle: something old, something new. *Frontiers in Plant Science* 25: 470.
- Munekage YN, Eymery F, Rumeau D, Cuiné S, Oguri M, Nakamura N, Yokota A, Genty B, Peltier G. 2010. Elevated expression of PGR5 and NDH-H in bundle sheath chloroplasts in C<sub>4</sub> *Flaveria* species. *Plant & Cell Physiology* 51: 664–668.
- Nakamura N, Iwano M, Havaux M, Yokota A, Munekage YN. 2013. Promotion of cyclic electron transport around photosystem I during the evolution of NADP-malic enzyme-type C<sub>4</sub> photosynthesis in the genus *Flaveria*. *New Phytologist* 199: 832–842.
- Ogawa T, Kobayashi K, Taniguchi YY, Shikanai T, Nakamura N, Yokota A, Munekage YN. 2023. Two cyclic electron flows around photosystem I differentially participate in C<sub>4</sub> photosynthesis. *Plant Physiology* 27: kiad032.
- Peltier G, Aro EM, Shikanai T. 2016. NDH-1 and NDH-2 plastoquinone reductases in oxygenic photosynthesis. *Annual Review of Plant Biology* 67: 55–80.
- Peterson RB, Schultes NP, McHale NA, Zelitch I. 2016. Evidence for a role for NAD(P)H dehydrogenase in concentration of CO<sub>2</sub> in the bundle sheath cell of *Zea mays*. *Plant Physiology* 171: 125–138.
- Raines CA. 2011. Increasing photosynthetic carbon assimilation in C<sub>3</sub> plants to improve crop yield: current and future strategies. *Plant Physiology* 155: 36–42.
- Shen L, Tang K, Wang W, Wang C, Wu H, Mao Z, An S, Chang S, Kuang T, Shen JR *et al.* 2022. Architecture of the chloroplast PSI–NDH supercomplex in *Hordeum vulgare*. *Nature* 601: 649–654.

- Shikanai T. 2014. Central role of cyclic electron transport around photosystem I in the regulation of photosynthesis. *Current Opinion in Biotechnology* 26: 25–30.
- Shikanai T. 2016. Chloroplast NDH: a different enzyme with a structure similar to that of respiratory NADH dehydrogenase. *Biochimica et Biophysica Acta* 1857: 1015–1022.
- Strand DD, Fishe N, Kramer DM. 2017. The higher plant plastid NAD(P)H dehydrogenase-like complex (NDH) is a high efficiency proton pump that increases ATP production by cyclic electron flow. *The Journal of Biological Chemistry* 292: 11850–11860.
- Strand DD, Livingston AK, Satoh-Cruz M, Froehlich JE, Maurino VG, Kramer DM. 2015. Activation of cyclic electron flow by hydrogen peroxide *in vivo*. *Proceedings of the National Academy of Sciences, USA* 112: 5539–5544.
- Su X, Cao D, Pan X, Shi L, Liu Z, Dall'Osto L, Bassi R, Zhang X, Li M. 2022. Supramolecular assembly of chloroplast NADH dehydrogenase-like complex with photosystem I from *Arabidopsis thaliana*. *Molecular Plant* 15: 454–467.
- Suorsa M. 2015. Cyclic electron flow provides acclimatory plasticity for the photosynthetic machinery under various environmental conditions and developmental stages. *Frontiers in Plant Science* 6: 800.
- Surpin M, Larkin RM, Chory J. 2002. Signal transduction between the chloroplast and the nucleus. *Plant Cell* 14: S327–S338.
- Takabayashi A, Kishine M, Asada K, Endo T, Sato F. 2005. Differential use of two cyclic electron flows around photosystem I for driving CO<sub>2</sub>-concentration mechanism in C<sub>4</sub> photosynthesis. *Proceedings of the National Academy of Sciences, USA* 102: 16898–16903.
- Tang QM, Huang YH, Ni XX, Lyu M-JA, Chen GY, Sage R, Zhu XG. 2022. Increased  $\alpha$ -ketoglutarate as a missing link from the C<sub>3</sub>–C<sub>4</sub> intermediate state to C<sub>4</sub> photosynthesis in the genus *Flaveria*. *BioRxiv*. doi: [10.1101/2022.06.01.494409](https://doi.org/10.1101/2022.06.01.494409).
- Thordal-Christensen H, Zhang Z, Wei Y, Collinge DB. 1997. Subcellular localization of H<sub>2</sub>O<sub>2</sub> in plants: H<sub>2</sub>O<sub>2</sub> accumulation in papillae and hypersensitive response during the barley–powdery mildew interaction. *The Plant Journal* 11: 1187–1194.
- Tsuchida H, Tamai T, Fukayama H, Agarie S, Nomura M, Onodera H, Ono K, Nishizawa Y, Lee BH, Hirose S *et al.* 2001. High level expression of C<sub>4</sub>-specific NADP-malic enzyme in leaves and impairment of photoautotrophic growth in a C<sub>3</sub> plant, rice. *Plant & Cell Physiology* 42: 138–145.
- Turkan I, Uzilday B, Dietz KJ, Bräutigam A, Ozgur R. 2018. Reactive oxygen species and redox regulation in mesophyll and bundle sheath cells of C<sub>4</sub> plants. *Journal of Experimental Botany* 69: 3321–3331.
- Wang L, Czedik-Eysenberg A, Mertz RA, Si Y, Tohge T, Nunes-Nesi A, Arrivault S, Dedow LK, Bryant DW, Zhou W *et al.* 2014a. Comparative analyses of C<sub>4</sub> and C<sub>3</sub> photosynthesis in developing leaves of maize and rice. *Nature Biotechnology* 32: 1158–1165.
- Wang P, Duan W, Takabayashi A, Endo T, Shikanai T, Ye JY, Mi H. 2006. Chloroplastic NAD(P)H dehydrogenase in tobacco leaves functions in alleviation of oxidative damage caused by temperature stress. *Plant Physiology* 141: 465–474.
- Wang Y, Bräutigam A, Weber AP, Zhu XG. 2014b. Three distinct biochemical subtypes of C<sub>4</sub> photosynthesis? A modelling analysis. *Journal of Experimental Botany* 65: 3567–3578.
- Yadav KN, Semchonok DA, Nosek L, Kouřil R, Fucile G, Boekema EJ, Eichacker LA. 2017. Supercomplexes of plant photosystem I with cytochrome b6f, light-harvesting complex II and NDH. *Biochimica et Biophysica Acta – Bioenergetics* 1858: 12–20.
- Yamori W, Sakata N, Suzuki Y, Shikanai T, Makino A. 2011. Cyclic electron flow around photosystem I via chloroplast NAD(P)H dehydrogenase (NDH) complex performs a significant physiological role during photosynthesis and plant growth at low temperature in rice. *The Plant Journal* 68: 966–976.
- Yamori W, Shikanai T. 2016. Physiological functions of cyclic electron transport around photosystem I in sustaining photosynthesis and plant growth. *Annual Review of Plant Biology* 67: 81–106.
- Zhao H, Wang Y, Lyu MA, Zhu XG. 2022. Two major metabolic factors for an efficient NADP-malic enzyme type C<sub>4</sub> photosynthesis. *Plant Physiology* 189: 84–98.
- Zhou H, Akçay E, Helliker BR. 2019. Estimating C<sub>4</sub> photosynthesis parameters by fitting intensive A/C<sub>i</sub> curves. *Photosynthesis Research* 141: 181–194.

## Supporting Information

Additional Supporting Information may be found online in the Supporting Information section at the end of the article.

**Dataset S1** Transcriptome data of maize *zmndf6* and *zmndhu* mutants.

**Dataset S2** Transcriptome data of rice *osndf6* and *osndhu* mutants.

**Dataset S3** Transcript abundance of photosynthetic genes in maize and rice *ndh* mutants.

**Dataset S4** Bundle sheath cell proteomics of maize wild-type and *zmndf6* mutant.

**Dataset S5** Metabolite analysis of maize and rice *ndh* mutants.

**Dataset S6** Summary of statistics.

**Dataset S7** Primers used in this study.

**Fig. S1** Schematic model and transcript levels of NDH subunits in maize and rice.

**Fig. S2** Mutation of *NDH* genes in maize and rice with CRISPR-Cas9 technology.

**Fig. S3** Phenotypes of maize *zmndf6* and *zmndhu* mutants growing in the field glasshouse.

**Fig. S4** Chlorophyll fluorescence induction kinetics and immunoblots of photosynthetic proteins.

**Fig. S5** Changes in bundle sheath cell protein content in maize *zmndf6* mutant.

**Fig. S6** Transcriptome analysis of maize and rice *ndh* mutants.

**Methods S1** Blue native-PAGE and Western blot.

**Methods S2** Transmission electron microscopy.

**Methods S3** Histological staining of reactive oxygen species accumulation.

**Methods S4** Paraffin section and I<sub>2</sub>–KI staining.

**Methods S5** Transcript abundance analysis.

**Methods S6** Separation of bundle sheath strands.

**Methods S7** Mass spectrometry analysis of protein samples.

**Table S1** Comparison of the BS : M ratio (mRNA or protein) of selected cyclic electron transport-related components in maize.

Please note: Wiley is not responsible for the content or functionality of any Supporting Information supplied by the authors. Any queries (other than missing material) should be directed to the *New Phytologist* Central Office.